RESEARCH MEMORANDUM

PRELIMINARY AERODYNAMIC INVESTIGATION OF THE EFFECT OF CAMBER ON A 60° DELTA WING WITH ROUND AND BEVELED LEADING EDGES

By John M. Riebe and Joseph E. Fikes

Langley Aeronautical Laboratory
Langley Air Force Base, Va.

NATIONAL ADVISORY COMMITTEE FOR AERONAUTICS

WASHINGTON

August 16, 1949

NACA RM L9F10

NATIONAL ADVISORY COMMITTEE FOR AERONAUTICS

RESEARCH MEMORANDUM

PRELIMINARY AERODYNAMIC INVESTIGATION OF THE EFFECT OF CAMBER ON A 60° DELTA WING WITH ROUND AND BEVELED LEADING EDGES

By John M. Riebe and Joseph E. Fikes

SUMMARY

An exploratory investigation to determine the aerodynamic effects of camber on a 60° apex delta-wing model has been conducted in the Langley 300 MPH 7- by 10-foot tunnel. Camber variation was accomplished through the deflection of full-span round and 25° beveled leading-edge flaps on a flat-sided triangular plan-form wing.

The maximum lift-drag ratio for the delta wing with no flap deflection was about 8.2 for both leading-edge shapes at a Reynolds number of 3×10^6. An increase up to 28 percent in lift-drag ratio occurred in the 0.2 to 0.3 lift-coefficient range for 20° flap deflections. Flap deflections resulted in small wing trim changes but did not greatly affect the longitudinal stability through the stall.

Deflecting the leading-edge flap to 30° reduced the maximum effective dihedral to about half the flap-neutral value and resulted in negative effective dihedral below lift coefficients of 0.3.

INTRODUCTION

It has been indicated from recent research on wing plan forms suitable for moderate supersonic flight that the low-speed longitudinal stability problems of the triangular plan-form wing appear to be less severe than for the conventional sweptback wing; because of its high taper and low aspect ratio, the triangular wing also has definite structural advantages over the conventional swept wings.

Theoretical calculations and experimental studies have shown that such wing plan forms will develop lift–drag ratios at supersonic Mach numbers which are sufficiently high for flight, being, however, generally lower than those of other plan forms. Low-speed research has also indicated poor landing characteristics of delta plan forms because of the relatively low lift–drag ratios, particularly in the high-lift condition.

The results of a theoretical study of triangular wings (reference 1) and a pressure-distribution investigation (reference 2) show that high loadings occur along the leading edge of triangular wings. These high loadings and their associated adverse pressure gradients result in separation over the leading-edge portion of the wing and develop vortices that flow back over the wing (references 1 to 5) even at relatively low lifts.

The present investigation made in the Langley 300 MPH 7- by 10-foot tunnel is a preliminary study aimed at increasing the low-speed lift–drag ratio by incorporating camber into a 60° delta wing. Camber was simulated for this investigation by deflecting full-span leading-edge flaps in an effort to reduce the high peak pressure along the leading edge and thus retard the separation effects. The configuration tested was chosen as the first attempt at solving this problem because it approaches a conical shape, which was believed to be efficient in unloading the leading edge, and because of its structural simplicity compared to other leading-edge flaps considered.

COEFFICIENTS AND SYMBOLS

The results of the tests are presented as standard NACA coefficients of forces and moments about the stability axes. Pitching-, yawing-, and rolling-moment coefficients are given about the wing 25-percent-mean-aerodynamic-chord point as shown in figure 1. The positive directions of forces and moments are shown in figure 2.

The coefficients and symbols are defined as follows:

C_L lift coefficient (L/qS)

C_D drag coefficient (D/qS)

C_Y lateral-force coefficient (Y/qS)

C_l rolling-moment coefficient (L'/qbS)

C_m pitching-moment coefficient ($M/q\bar{c}S$)

C_n yawing-moment coefficient (N/qbS)

L lift, pounds (-Z)

D drag (-X when $\Psi = 0$), pounds

X force along X-axis, pounds

Y force along Y-axis, pounds

Z force along Z-axis, pounds

L' rolling moment, foot-pounds

M pitching moment, foot-pounds

N yawing moment, foot-pounds

q free-stream dynamic pressure, pounds per square foot $\left(\frac{1}{2}\rho V^2\right)$

S wing area (3.67 sq ft)

$\bar{c}$ wing mean aerodynamic chord (M.A.C.) (1.68 ft) $\left(\frac{2}{S}\int_0^{b/2} c^2 dy\right)$

b wing span (2.91 ft)

V free-stream velocity

R Reynolds number

δ_n leading-edge flap deflection measured perpendicular to hinge line, degrees

α angle of attack of wing with respect to chord plane at root of model, degrees

c local wing chord, foot

y lateral distance from plane of symmetry, measured parallel to Y-axis, feet

$$C_{l_\psi} = \left(\frac{\partial C_l}{\partial \psi}\right)_\alpha$$

$$C_{n_\psi} = \left(\frac{\partial C_n}{\partial \psi}\right)_\alpha$$

$$C_{Y_\psi} = \left(\frac{\partial C_Y}{\partial \psi}\right)_\alpha$$

$$C_{L_\alpha} = \left(\frac{\partial C_L}{\partial \alpha}\right)_\psi$$

The subscripts α and ψ indicate the factor held constant.

APPARATUS AND MODEL

The model was tested in the Langley 300 MPH 7- by 10-foot tunnel on a single strut as shown in figure 3.

The general arrangement of the 60° delta-wing model with round and beveled leading edges is shown in figure 1. The wing had a 60° apex angle and the aspect ratio was 2.31. The model was made from a flat steel plate 1/2 inch thick and had a fixed beveled trailing edge with an included angle of 10°. The flat airfoil was used because of simple construction, and, because of the preliminary aspect of the investigation, it was felt that a flat plate would suffice. The model was interchangeably equipped with either a 0.25-inch radius or a beveled leading-edge flap with an included angle of 25°. Each leading-edge flap was attached to the main body of the model by means of a brass strip in the lower surface of the wing which also served as a hinge. For the flap-deflected condition, the upper-surface gap between the flap and the wing was filled with wax to a circular contour which was tangent to the surface of the flap and the wing.

TESTS

Test Conditions

The tests were made in the Langley 300 MPH 7- by 10-foot tunnel at dynamic pressures of approximately 25 and 100 pounds per square foot, corresponding to airspeeds of about 100 and 200 miles per hour. Reynolds numbers for these airspeeds, based on the mean aerodynamic chord (1.68 ft) of the 60° delta wing, were approximately 1.5×10^6 and 3.0×10^6, respectively. Corresponding Mach numbers were 0.13 and 0.27. The tests were run throughout a range of angles of attack of 0° to 40°, and through a −5° to 20° yaw range.

Corrections

Blocking, jet-boundary, and air-stream-inclination corrections have been applied to the data. The jet-boundary corrections were obtained from methods outlined in reference 6. These corrections are strictly applicable only to wings of larger span and aspect ratio. However, it is believed that the error in using these corrections for the present setup is negligible. The effects of the support strut, which were determined by using an image system, have been subtracted from the data; no tares for the effects of yaw have been applied to the yaw data.

RESULTS AND DISCUSSION

The aerodynamic characteristics in pitch of the 60° delta-wing model with round and beveled leading-edge flaps are presented in figures 4 and 5, respectively; lift-drag ratios are presented in figures 6 and 7. The original data for $\delta_n = 0°$ (fig. 4(a)) were rejected because of extremely large scatter of the test data resulting from temporary malfunction of the wind-tunnel scale system. The test was later rerun for only part of the angle-of-attack range as shown. Aerodynamic characteristics in yaw are given in figures 8 and 9, and lateral-stability parameter variations with lift coefficient are given in figures 10 and 11. Longitudinal and lateral-stability parameters determined at a Reynolds number of 3.0×10^6 are presented in table I.

Lift

Leading-edge flaps undeflected.— The lift-curve slopes near zero lift coefficient for the 60° delta wing with round leading edge and beveled leading edge, $\delta_n = 0°$, were 0.046 and 0.044, respectively, at a Reynolds number of 3.0×10^6. (See figs. 4(b) and 5(b).) These values agreed closely with slopes predicted by Krienes theory for low-aspect-ratio highly tapered wings (fig. 5 of reference 1) and with results from other tests on similar plan-form wings (references 4 and 5). As with other highly swept low-aspect-ratio wings, the lift-curve slope was greater in the middle part of the angle-of-attack range because of more rapid loading at the tips resulting from strong lateral flow (reference 2). The maximum lift coefficient for the round leading-edge airfoil, $\delta_n = 0°$, was about 1.28, occurring at about 33° angle of attack. The beveled leading-edge airfoil, $\delta_n = 0°$, had a maximum lift coefficient which was slightly less, about 1.22 at a Reynolds number of 3.0×10^6. The Reynolds number range covered in the present investigation, 1.5×10^6 to 3×10^6, affected $C_{L_{max}}$ only slightly. The similarity in $C_{L_{max}}$ for the two nose shapes at the Reynolds numbers of the present investigation may not hold at full-scale Reynolds numbers, because vortex flow caused by leading-edge separation occurs at both high and low Reynolds numbers over sharp leading-edge delta wings but only at low Reynolds numbers over round leading-edge delta wings. (See references 3, 5, and 7.) The manner in which separation results in the occurrence of vortices is discussed in detail in references 3 and 5. In essence, however, the vortices maintain the lift to higher angles of attack by delaying trailing-edge separation. Because round leading-edge delta wings do not exhibit leading-edge separation at high Reynolds numbers, lower maximum lift coefficients occur.

Leading-edge flaps deflected.— Deflecting the leading-edge flaps resulted in a progressive decrease in slope of the lift curve for both leading-edge conditions. The change in angle-of-zero lift with flap deflection was as would be expected since deflection of leading-edge flaps results in essentially a decrease in angle of attack. Although flap deflection resulted in a decrease in lift at all angles of attack, the wing with flap deflected gave about the same maximum lift coefficient as the plain wing. Large-scale tests on a 60° delta wing with biconvex airfoil sections (reference 8) indicated increases in maximum lift coefficient with deflection of leading-edge flaps extending almost full span with a large portion of the flap area near the apex. Practically no increases in maximum lift coefficient up to 20° deflection and large decreases after 20° deflection occurred for flap deflection confined to the region of the apex.

Lift-drag ratios.- Leading-edge flap deflections up to 60° resulted in a progressive decrease in lift coefficient at a given angle of attack below the stall, and for flap deflections up to 30°, resulted in decreases in drag coefficient. The proportional reductions in drag, however, were greater than the proportional reductions in lift at low angles of attack, resulting in an increase of lift-drag ratio at low-lift coefficients. (See figs. 6 and 7.) The maximum increase in lift-drag ratio was about 28 percent, occurring in the 0.2 to 0.3 lift-coefficient range; L/D was about 8.2 for the wing with both round and beveled leading-edge flaps at 0° and about 10.5 for the optimum flap deflection, 20° for both leading edges at a Reynolds number of 3×10^6. The maximum values of L/D were not critically dependent upon flap deflection in the 10° to 30° flap-deflection range and were generally about the same for both leading-edge shapes. However, flap deflections of 40° and greater had lift-drag ratios which were generally lower than those of the plain wing. The values of L/D for the present investigation were lower than those obtained in other investigations at high Reynolds numbers. (See references 4 and 7.) However, according to reference 4, increasing Reynolds number resulted in an increase in lift-drag ratio because of skin-friction drag-coefficient decrease. The lift-drag ratios of reference 4 are acknowledged to be higher than those of reference 7, probably because of the method of testing. If the trend of the curves with Reynolds number is considered (decrease in L/D ratio with decrease in Reynolds number) with the lower lift-drag ratios of other delta-wing data (reference 7), the lift-drag ratios for the wing of the present investigation are of the right order of magnitude. For several deflections of the beveled leading-edge flap, higher maximum lift-drag ratios were obtained at lower Reynolds number. (See fig. 7.) It is not known why the effect of Reynolds number on lift-drag ratio is different from that shown in reference 4 and from that of the round leading-edge delta wing. (See fig. 6.)

Theoretical considerations (reference 1) and pressure distributions (reference 2) indicate that delta-wing plan forms have high negative peak pressures along the leading edge and span-load distributions of elliptical shape, resulting in minimum induced drag. As mentioned previously, separation and vortex flow originating at the apex occur over the upper surface of the delta wing through a large part of the lift-coefficient range. This results in increased turbulence and profile drag. Although the vortex type of flow is necessary at high angles of attack to delay trailing-edge separation and thus maintain high maximum lift coefficients (reference 3), the vortices are unnecessary at lower angles of attack. The effect of the leading-edge flaps in increasing the lift-drag ratio (indicated in the present tests at low angles of attack), probably resulted from alleviation of the leading-edge separation and the resulting vortices, thereby giving a

reduction in turbulence and profile drag. Somewhat similar conclusions were reported in reference 9, where larger lift–drag ratios were obtained by adding camber to a circular plate and were attributed to a reduction of vortex separation.

The induced drag was already near minimum for 0° flap deflection (references 1 and 2), so any reduction of drag caused by a span loading more nearly elliptical was probably small. Evidently, the proportional reduction in the profile–drag part of the lift–drag ratio was larger than the proportional decrease in lift which resulted from the reduction of the high peak pressures along the leading edge. At present, these theories lack experimental verification. Reynolds number will also affect the angle of attack at which leading–edge separation first occurs; the characteristics of camber in increasing L/D may therefore be different on full–scale models as was shown in reference 8.

Air–flow studies.– In order to evaluate the reduction and delay of vortex separation over the delta wing with flap deflection, additional tests were made in the form of boundary–layer flow studies, using lampblack and benzine on the wing with beveled leading–edge flap undeflected and deflected 20°. (See fig. 12.) The patterns shown are believed to be those produced by the bottom of the vortex flow (described in references 3 and 5) in contact with the surface of the model. The majority of the flow photographs were taken after the benzine had evaporated or had been blown from the model leaving a trace of the boundary air flow in the lampblack. However, in some cases where the vortex pattern was more clearly indicated during evaporation there are two photographs at a given angle of attack; the partial–evaporation photograph always precedes the complete–evaporation photograph. The portion of the lampblack–benzine coating on the wing affected by the vortex flow was always the first to evaporate, as shown in the first photograph of some of the sets, (for example $\alpha = 8°$, fig. 12); this early evaporation would be very unlikely if the pattern indicated on the photographs was merely cross flow. Vortices were also indicated by probing the model with a wool streamer. The streamer would rotate in and near the region of vortices indicated by the lampblack tests and in a direction toward the wing tip near the surface of the model. The height of the vortices was indicated to be such that the core would be on a line above the wing surface, when viewed from the side, at an angle approximately equal to one–third the angle of attack, similar to that shown in reference 5.

In figure 12, with flaps undeflected, the vortex pattern is very slight at $\alpha = 3°$; and at $\alpha = 5°$ (the angle of attack of maximum L/D, flaps 0) the vortex becomes quite evident. As the value of α is increased, the outline of the vortices becomes wider and the inner boundary moves inward to the center of the model. With flaps

deflected 20°, the start of the vortex was delayed to an angle of attack of about 8°. After the vortex began, its progression was very similar to the vortices progression at the lower angles of attack with flaps undeflected. Comparison of the two flap deflections at a given angle of attack indicates a larger vortex for the flap-undeflected condition.

The results shown with the lampblack and benzine tests agree closely with the tuft studies shown in figures 13(a) and 13(b). In figure 13(a), with the flaps undeflected, the flow first became rough at about 2° near the apex and then the roughness spread along the leading edge and progressed inward to the center of the model as the angle of attack was increased. This rough air is attributed to partial separation and the vortex flow. The stall first occurred at the tips at or near an angle of attack of 27° and spread along the leading edge and inward from the tips until the model was completely stalled at $\alpha = 38°$.

In figure 13(b), with the flaps deflected to 30°, the onset of the rough air flow was delayed to an angle of attack of 7°, where it first occurred along the leading edge near the apex of the model. These results agree with those obtained from the lampblack tests in that the camber delays the partial separation and the occurrence of turbulent vortices to a higher angle of attack. From the angle of attack where the rough air flow first occurred, the pattern of rough air and stall progression was similar to the pattern with flaps undeflected, with complete stall at $\alpha = 38°$.

It appears from the results of the force, lampblack, and tuft tests that improvement in lift-drag ratio may also be provided at higher lift coefficients by delaying the start of the vortices to still higher lift coefficients up to the angle of attack at which they are necessary to prevent trailing-edge stall. The delay might be obtained by introduction of camber in the wing leading-edge flaps combined with more flap area in the region of the apex. Higher lift-drag ratios at maximum lift might be obtained by using slots to prevent trailing-edge stall and eliminate the apex vortices throughout the entire lift range.

Longitudinal Stability

The pitching-moment curves of figures 4 and 5 generally did not show irregularities as severe as those found for delta-wing models at high Reynolds numbers and high angles of attack (references 5 and 7); the separation on the subject wing started more gradually and was not as abrupt as that indicated for the reference wings.

The model was longitudinally stable up through the stall angle for both nose shapes and all flap deflections, a characteristic generally found on delta-wing models. Deflecting the flaps with either nose shape, varied the slope of the pitching-moment-coefficient curve only slightly and resulted in positive increments in pitching moment. However, the flaps would be unsatisfactory as a trim device because of the small increments and because of irregular and reversed effectiveness for large deflections. The small positive increments in pitching moment with flap deflection probably resulted from an unloading of the leading-edge flaps; this unloading was more effective at the rear part of the wing where the flap area was larger. With some alterations, such as increased flap area near the apex, it may be possible to design a flap giving no trim change.

Lateral Stability

The aerodynamic characteristics of the delta wing in yaw showed only small variation with flap leading-edge shape but generally large effects of flap deflection. (See figs. 8 to 11.) The lateral-stability coefficients varied fairly linearly with angle of yaw at 10° angle of attack (figs. 8 and 9) and did not drop off in the yaw range tested.

As is the usual case for highly swept wings of high taper, large changes in the effective dihedral C_{l_ψ} occurred throughout the lift range (figs. 10 and 11); the parameters were determined in the −5° to 5° yaw range. Negative effective dihedral was present at lift coefficients above 1.04 for the wing with round leading-edge flap at 0°. The values of C_{l_ψ} for the delta wing with beveled leading-edge flap flap at 0° varied in a manner similar to those for the round leading-edge wing except that the maximum value of C_{l_ψ} was less and negative effective dihedral occurred at a lower lift coefficient (0.92). Deflection of the nose flaps to 30° reduced the effective dihedral throughout the lift range for both leading-edge shapes. The maximum positive effective dihedral for the wing with 30° leading-edge flap deflection was about half that of the 0° flap-deflection condition and occurred at higher angles of attack.

The directional stability of the delta wing, as determined by C_{n_ψ}, was about the same with or without camber throughout the lift range and increased slightly with lift coefficient up to about $C_L = 0.8$.

The parameter C_{Y_ψ} increased uniformly with lift coefficient for the delta wing with no camber. The variation of C_{Y_ψ} with lift coefficient for both leading-edge shapes deflected 30° showed a decrease up to about the middle of the lift range and then showed a large increase with lift coefficient.

CONCLUSIONS

The results of tests in the Langley 300 MPH 7- by 10-foot tunnel to determine the effect of camber on a flat-plate 60° apex-angle delta wing accomplished by deflection of full-span round and beveled leading-edge flaps indicated the following conclusions:

1. In the 0.2 to 0.3 lift-coefficient range, up to 28 percent increase in lift-drag ratio was obtained for a 20° deflection of either the beveled or round leading-edge flap.

The values of lift-drag ratio were not critically dependent upon flap deflections in the range from 10° to 30°.

2. The values of $C_{L_{max}}$ were almost independent of nose-flap deflection. The angle of attack for maximum lift increased with flap deflection.

3. Flap deflections resulted in small trim changes but did not greatly affect the longitudinal stability.

4. Flap deflections did not vary the slight amount of directional stability inherent in the delta-wing model but reduced the effective dihedral.

Langley Aeronautical Laboratory
National Advisory Committee for Aeronautics
Langley Air Force Base, Va.

REFERENCES

1. Jones, Robert T.: Properties of Low-Aspect-Ratio Pointed Wings at Speeds below and above the Speed of Sound. NACA Rep. 835, 1946.

2. Wick, Bradford H.: Chordwise and Spanwise Loadings Measured at Low Speed on a Triangular Wing Having an Aspect Ratio of Two and an NACA 0012 Airfoil Section. NACA TN 1650, 1948.

3. Wilson, Herbert A., Jr., and Lovell, J. Calvin: Full-Scale Investigation of the Maximum Lift and Flow Characteristics of an Airplane Having Approximately Triangular Plan Form. NACA RM L6K20, 1947.

4. Edwards, George G., and Stephenson, Jack D.: Tests of a Triangular Wing of Aspect Ratio 2 in the Ames 12-Foot Pressure Wind Tunnel. I - The Effect of Reynolds Number and Mach Number on the Aerodynamic Characteristics of the Wing with Flap Undeflected. NACA RM A7K05, 1947.

5. Anderson, Adrien E.: An Investigation at Low Speed of a Large-Scale Triangular Wing of Aspect Ratio Two. - II. The Effect of Airfoil Section Modifications and the Determination of the Wake Downwash. NACA RM A7H28, 1947.

6. Gillis, Clarence L., Polhamus, Edward C., and Gray, Joseph L., Jr.: Charts for Determining Jet-Boundary Corrections for Complete Models in 7- by 10-Foot Closed Rectangular Wind Tunnels. NACA ARR L5G31, 1945.

7. Anderson, Adrien E.: An Investigation at Low Speed of a Large-Scale Triangular Wing of Aspect Ratio Two. - I. Characteristics of a Wing Having a Double-Wedge Airfoil Section with Maximum Thickness at 20-Percent Chord. NACA RM A7F06, 1947.

8. Whittle, Edward F., Jr., and Lovell, J. Calvin: Full-Scale Investigation of an Equilateral Triangular Wing Having 10-Percent-Thick Biconvex Airfoil Sections. NACA RM L8G05, 1948.

9. Winter, H.: Flow Phenomena on Plates and Airfoils of Short Span. NACA TM 798, 1936.

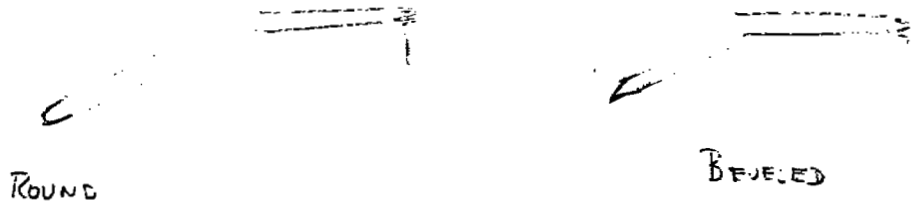

TABLE I

LONGITUDINAL- AND LATERAL-STABILITY PARAMETERS FOR DELTA WING WITH ROUND AND BEVELED LEADING-EDGE FLAPS

[$R \approx 3.0 \times 10^6$]

Leading edge	δ_n (deg)	[a] $\partial C_L/\partial\alpha$	[a] $\partial C_m/\partial C_L$	[b] $\partial C_l/\partial\psi$	[b] $\partial C_n/\partial\psi$	[b] $\partial C_Y/\partial\psi$
Round	0	0.046	−0.086	0.0019	−0.0003	0.0015
Round	30	.041	−.086	0	−.0003	.0017
Beveled	0	.044	−.082	.0014	−.0003	.0006
Beveled	30	.039	−.095	.0002	−.0003	.0014

[a] $\psi = 0$

[b] $\alpha = 10°$

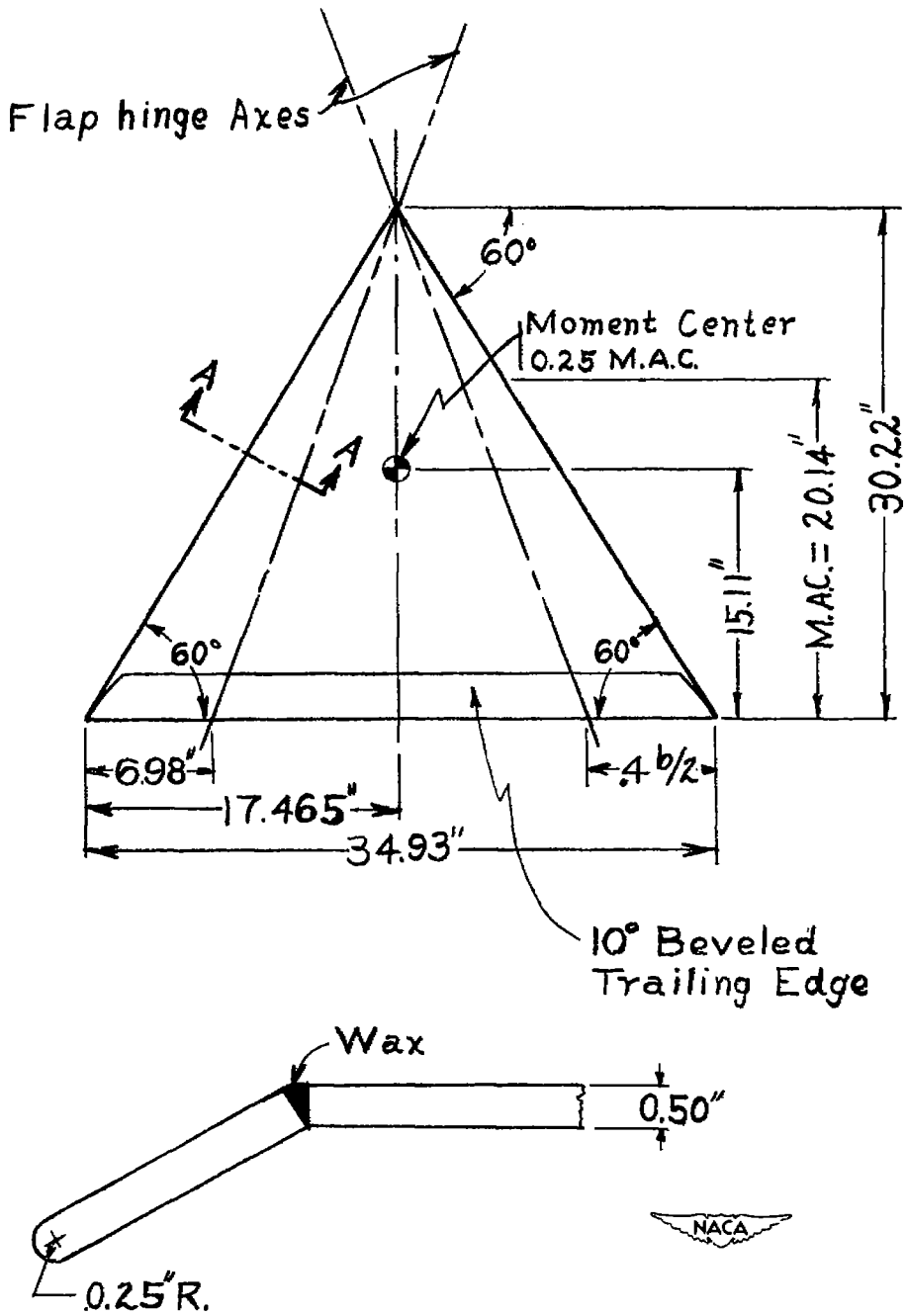

(a) Round leading-edge flaps.

Figure 1.– General arrangement of 60° delta wing model.

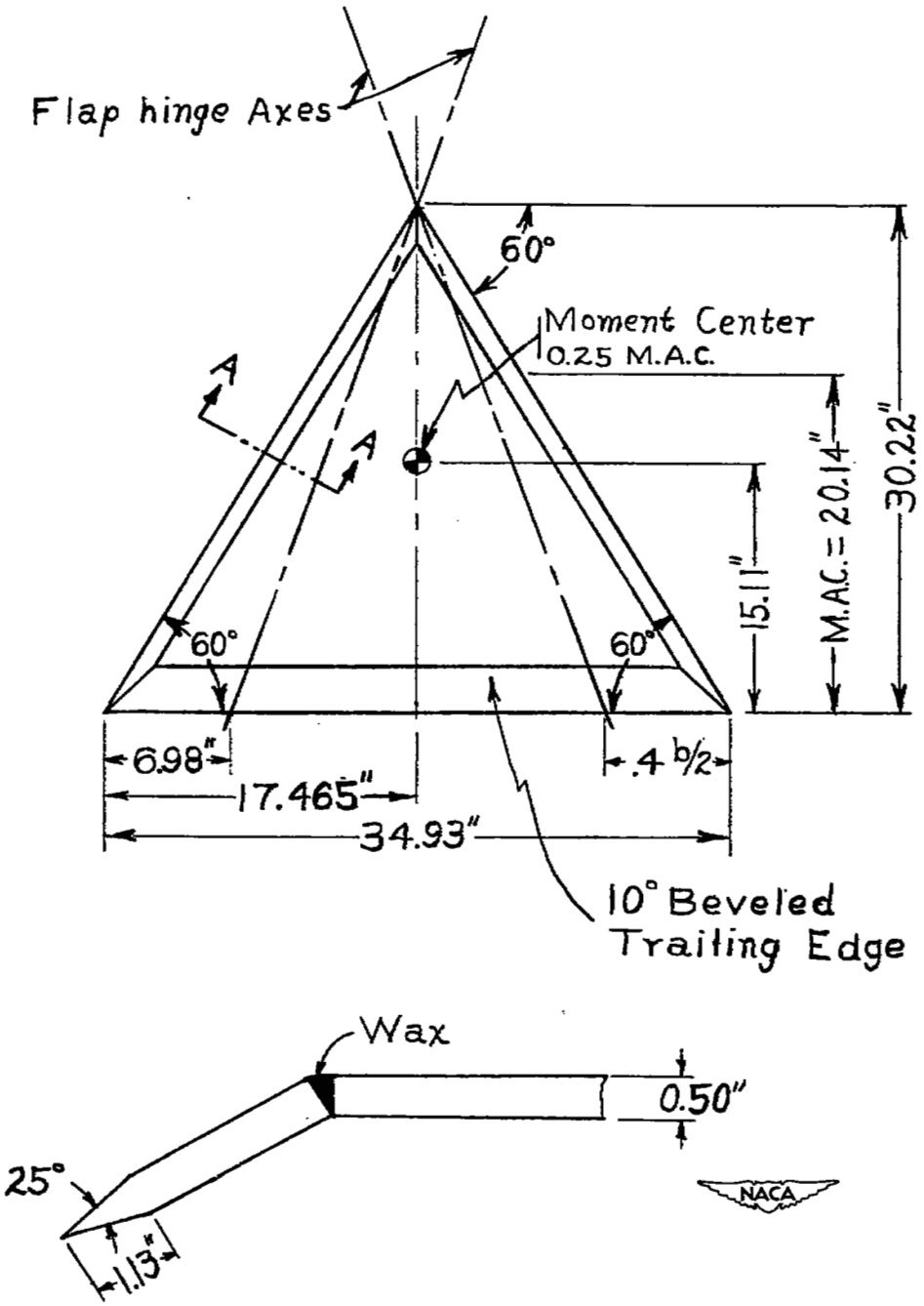

(b) Beveled leading-edge flaps.

Figure 1.– Concluded.

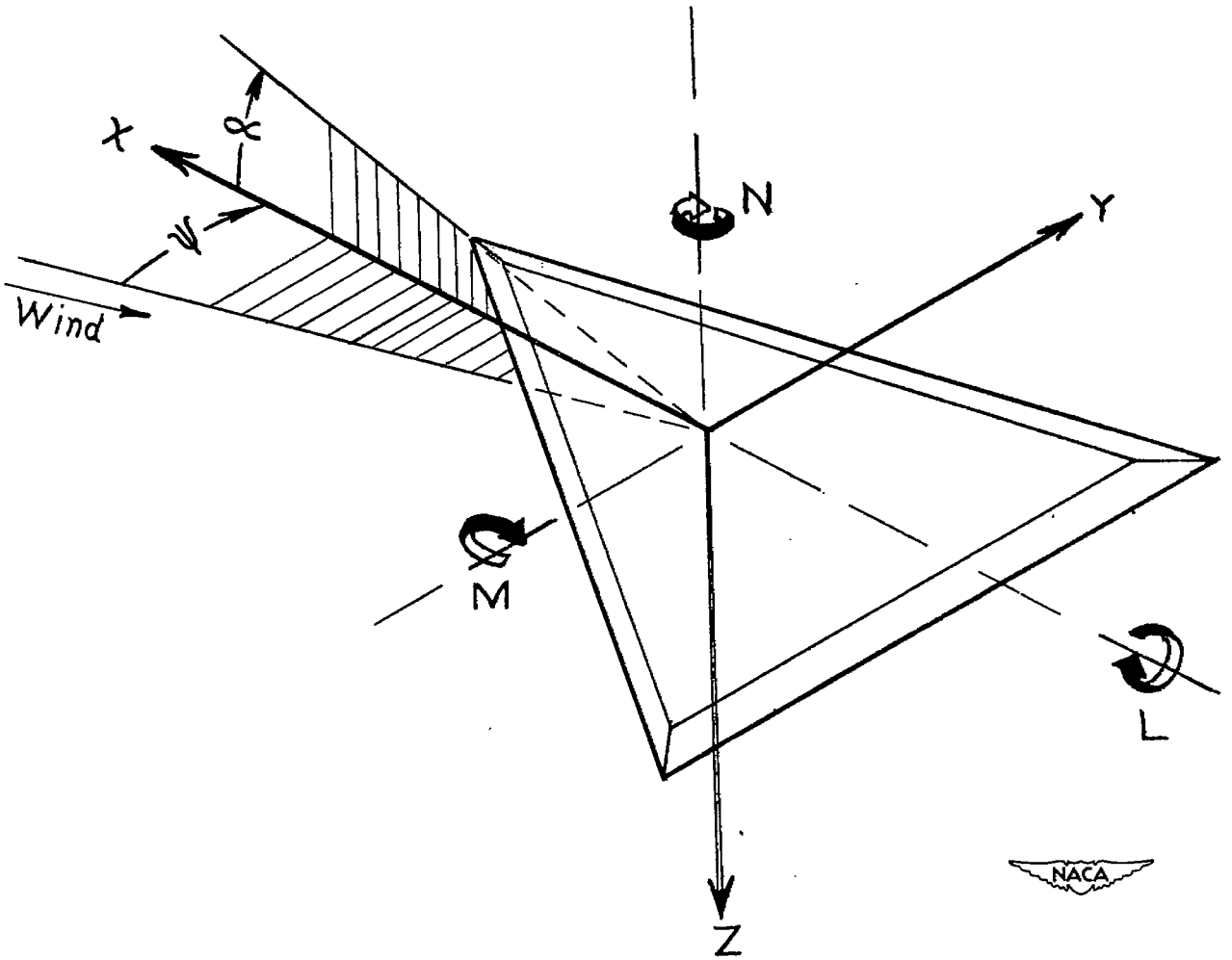

Figure 2.— System of stability axes. Positive values of forces, moments, and angles are indicated by arrows.

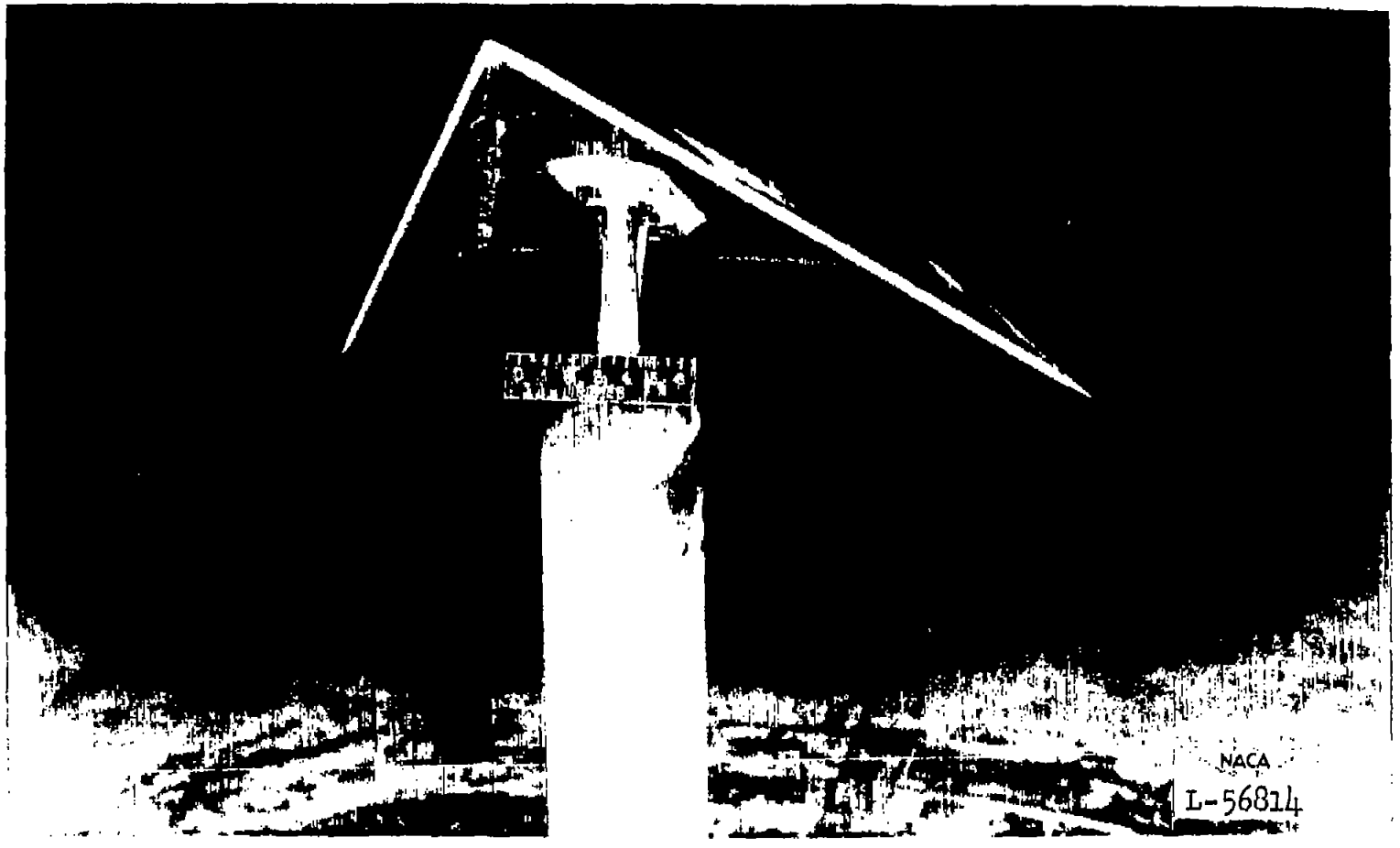

(a) Front view.

Figure 3.- The 60° delta-wing model with full-span round leading-edge flaps deflected 30°, mounted in the Langley 300 MPH 7- by 10-foot wind tunnel.

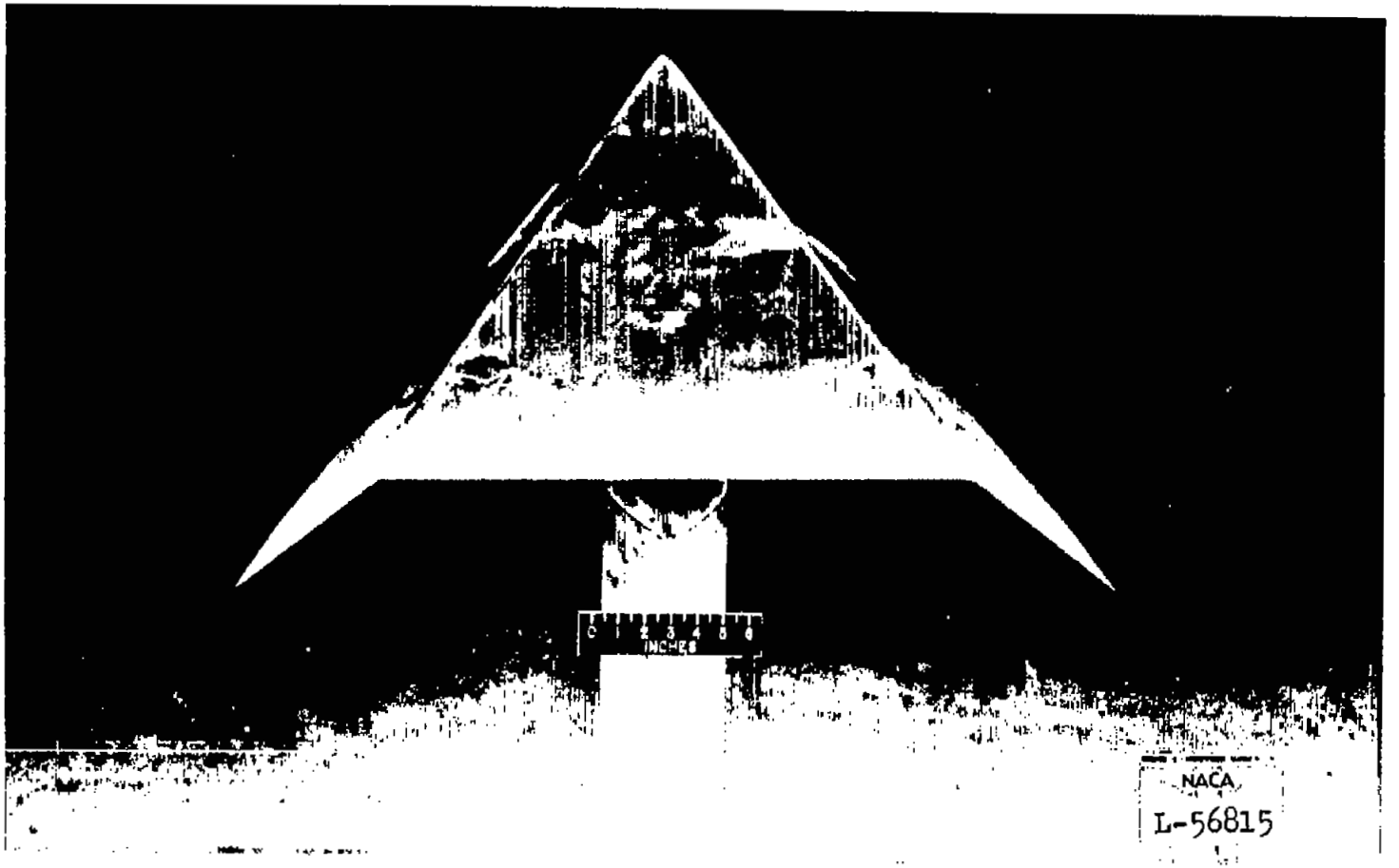

(b) Rear view.

Figure 3.- Concluded.

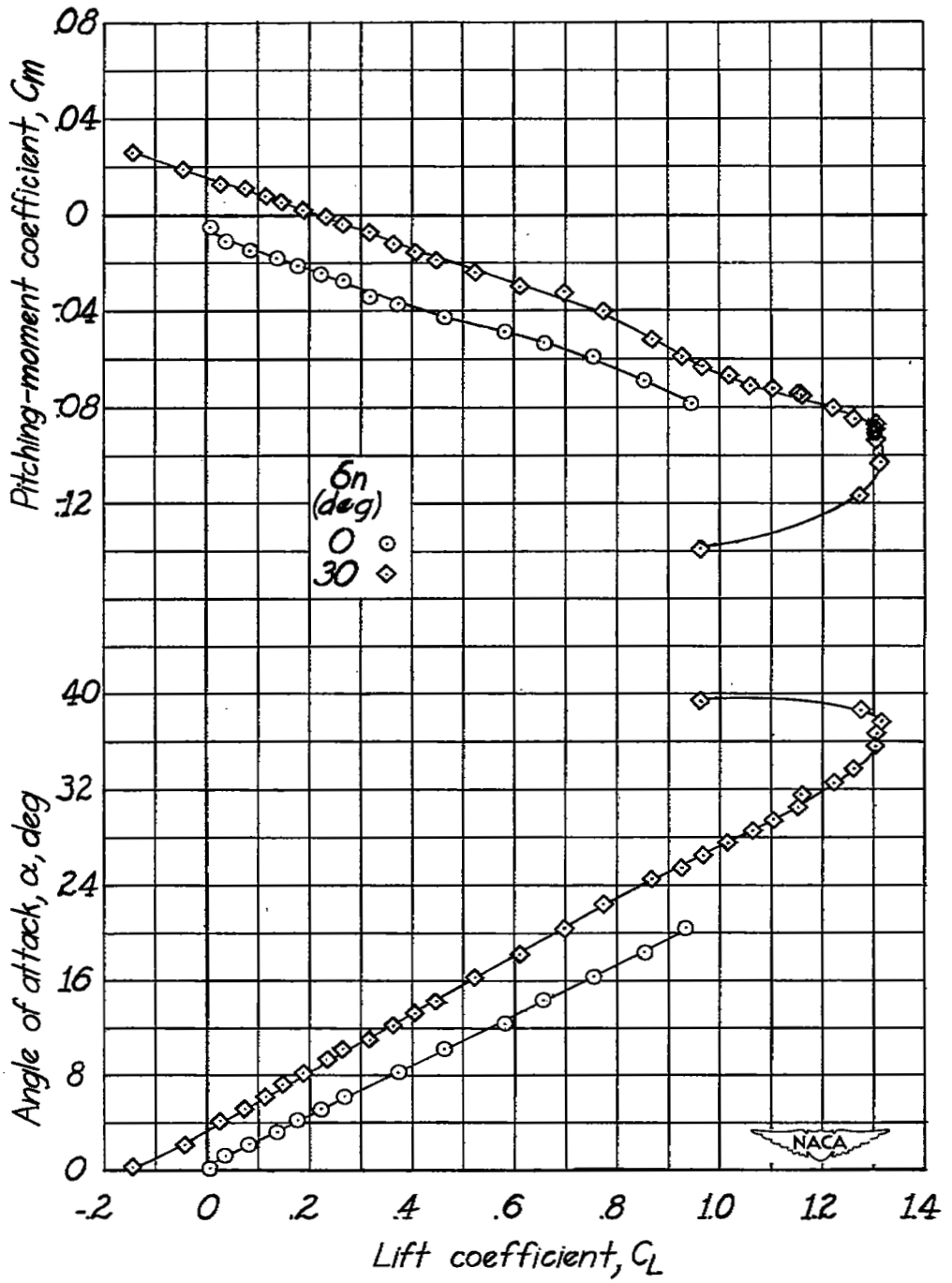

(a) $R \approx 1.5 \times 10^6$.

Figure 4.– Aerodynamic characteristics in pitch of 60° delta wing with full-span round leading-edge flaps.

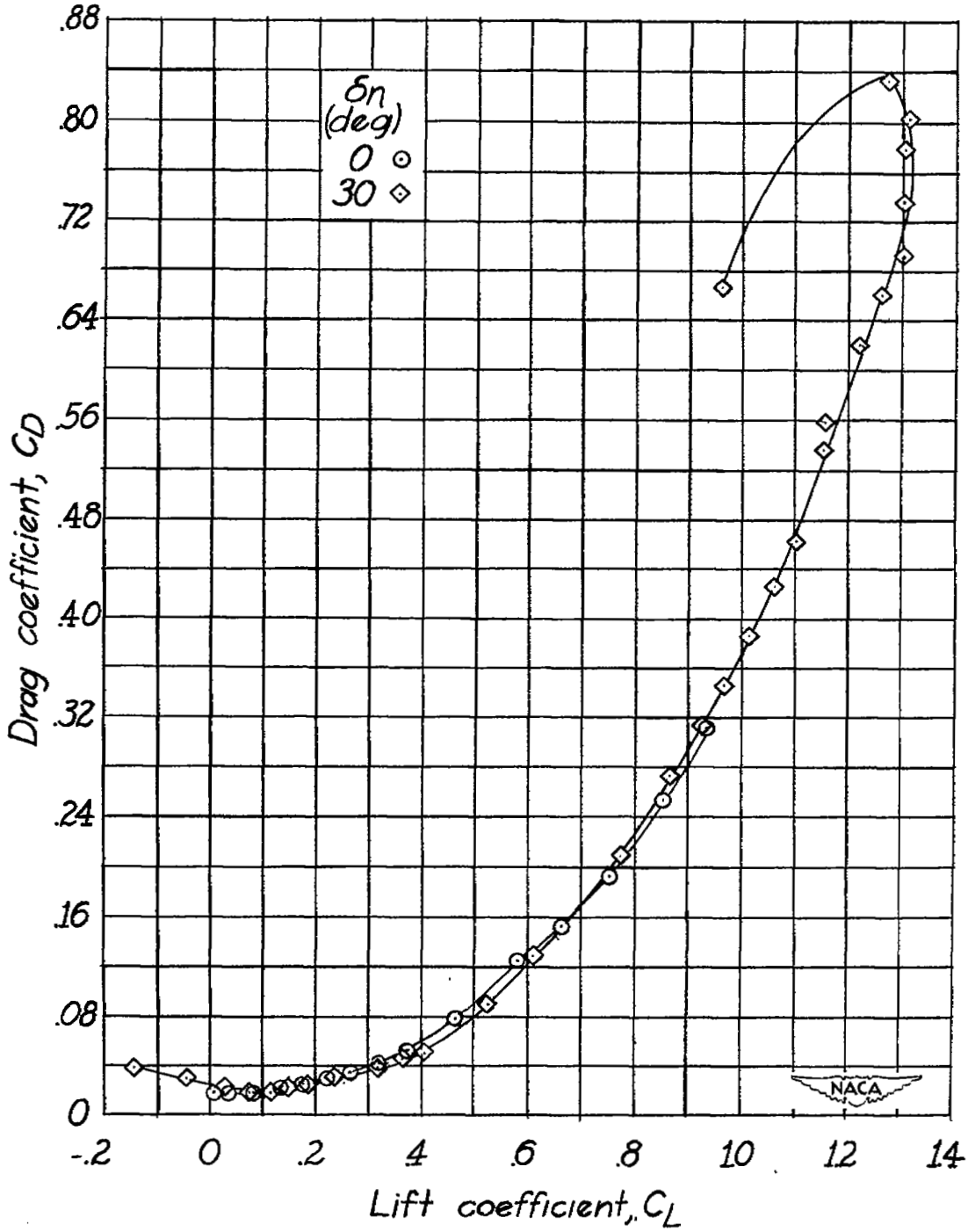

(a) Concluded.

Figure 4.– Continued.

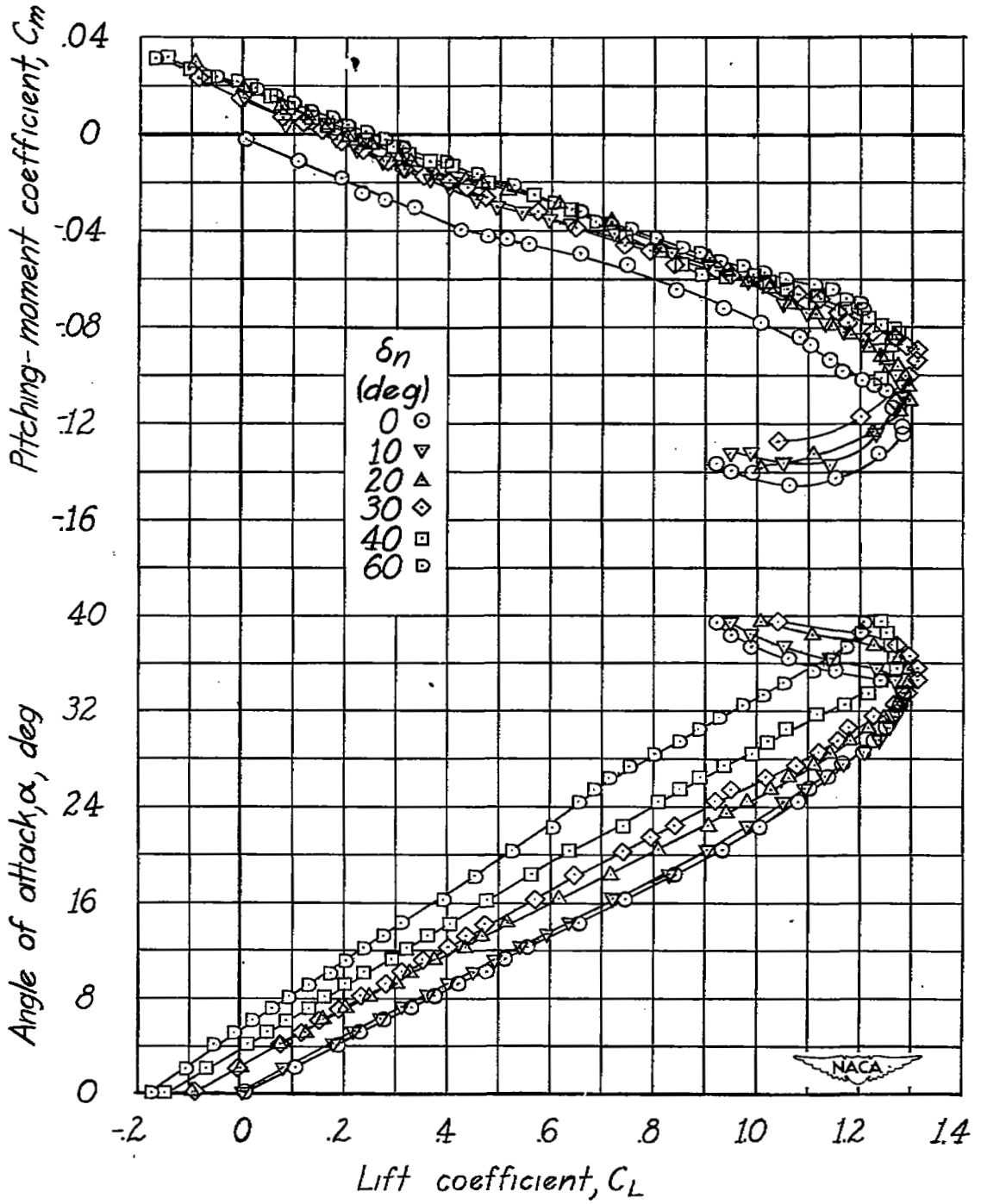

(b) $R \approx 3.0 \times 10^6$.

Figure 4.— Continued.

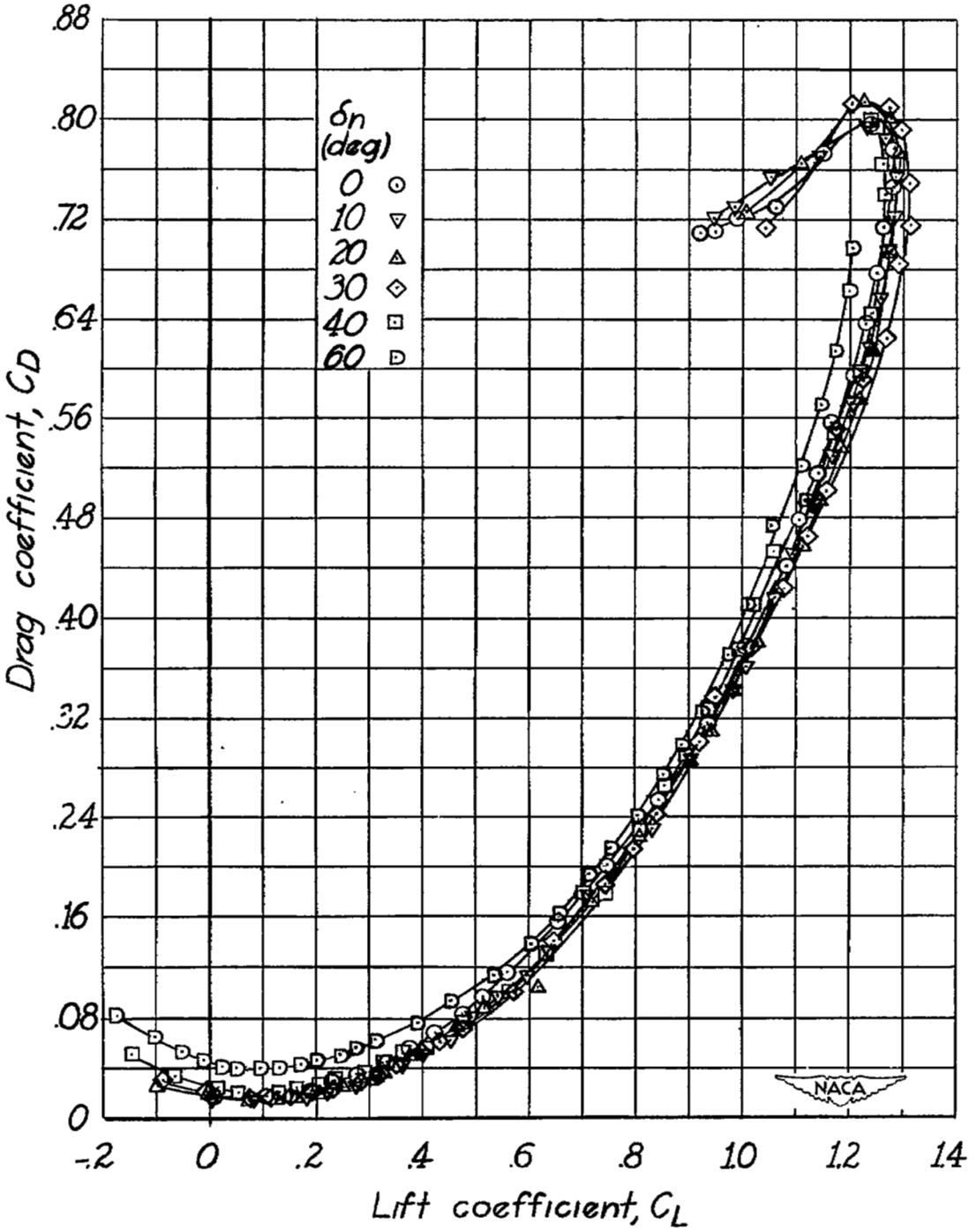

(b) Concluded.

Figure 4.– Concluded.

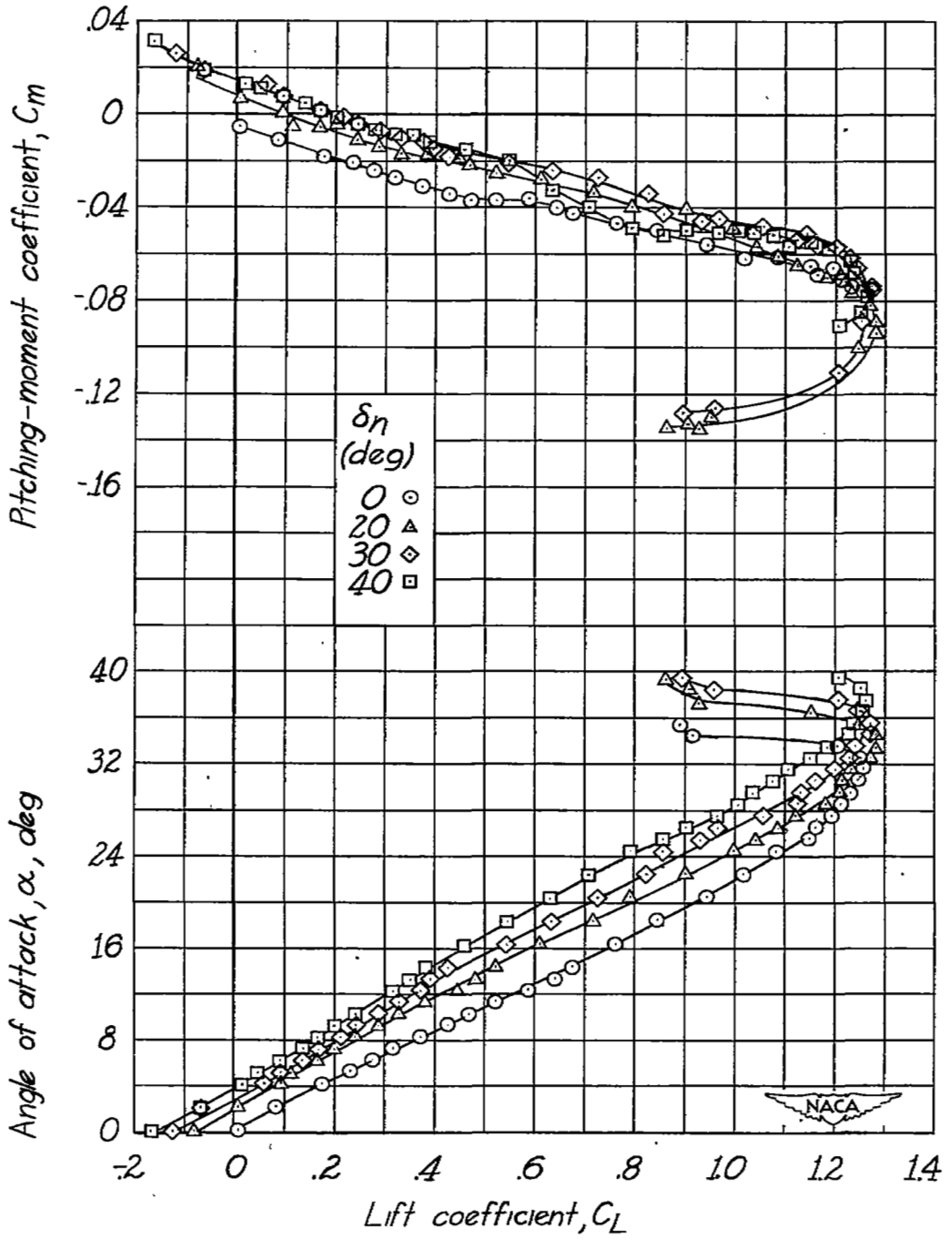

(a) $R \approx 1.5 \times 10^6$.

Figure 5.– Aerodynamic characteristics in pitch of 60° delta wing with full-span beveled leading-edge flaps.

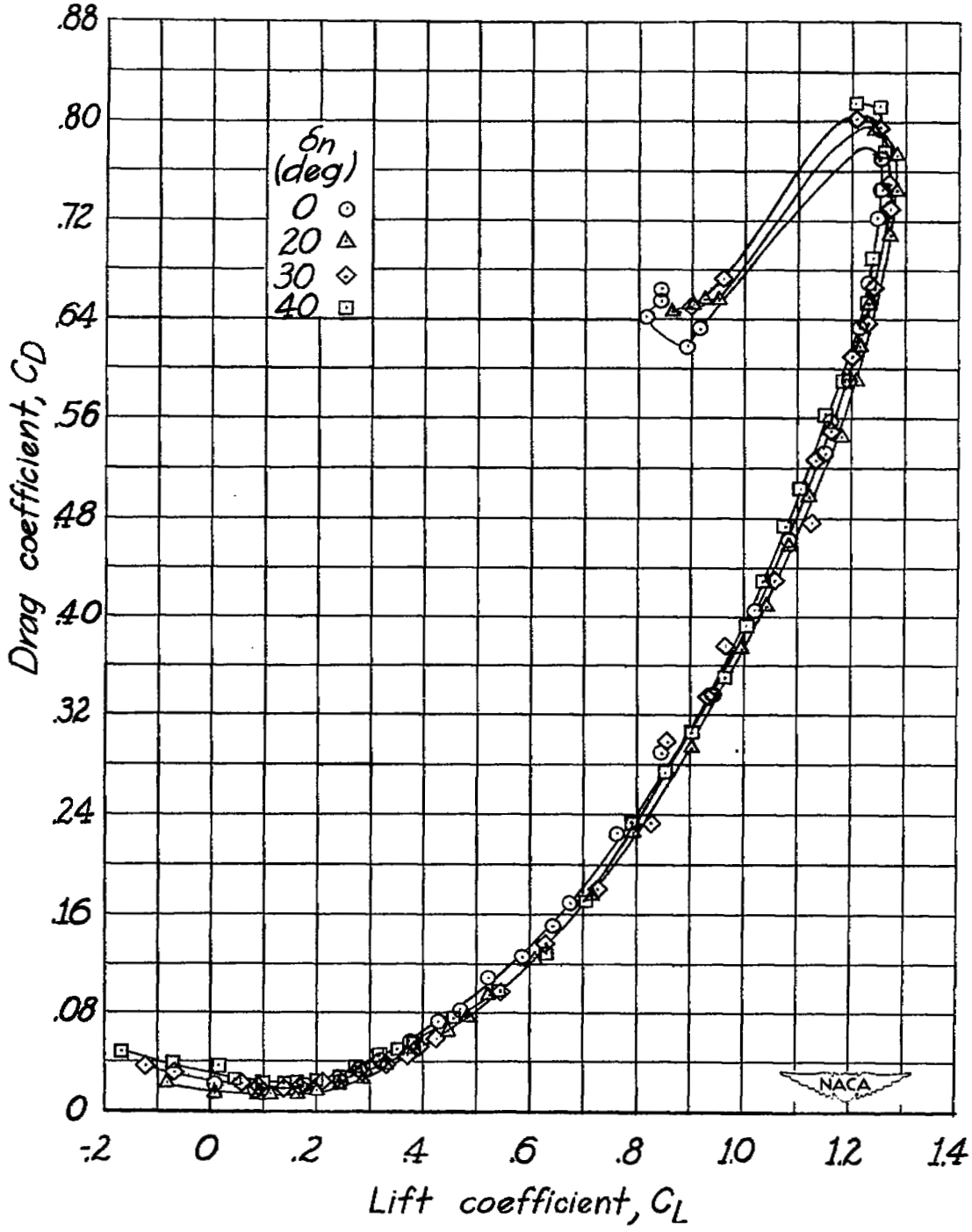

(a) Concluded.

Figure 5.– Continued.

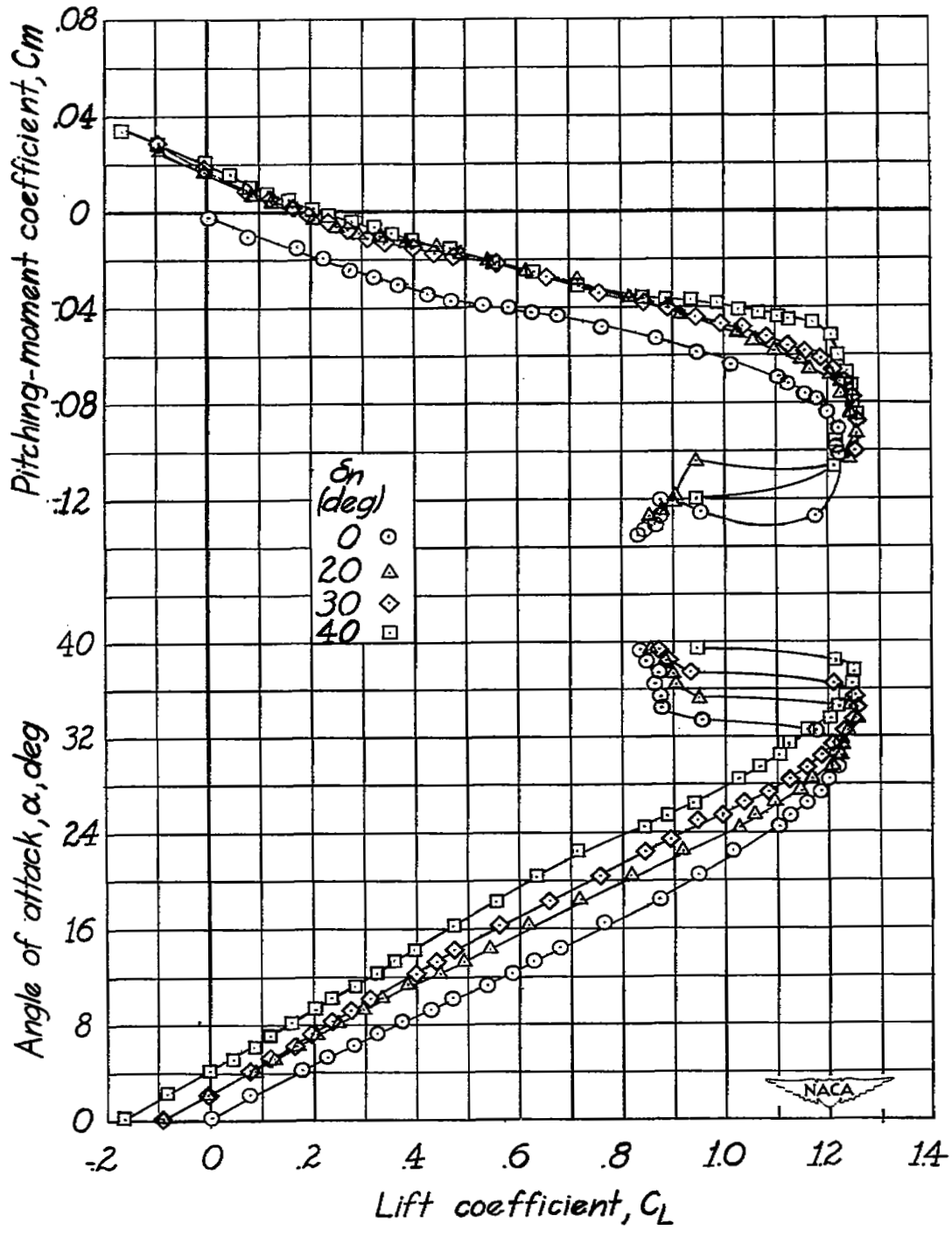

(b) R ≈ 3.0×10^6.

Figure 5.– Continued.

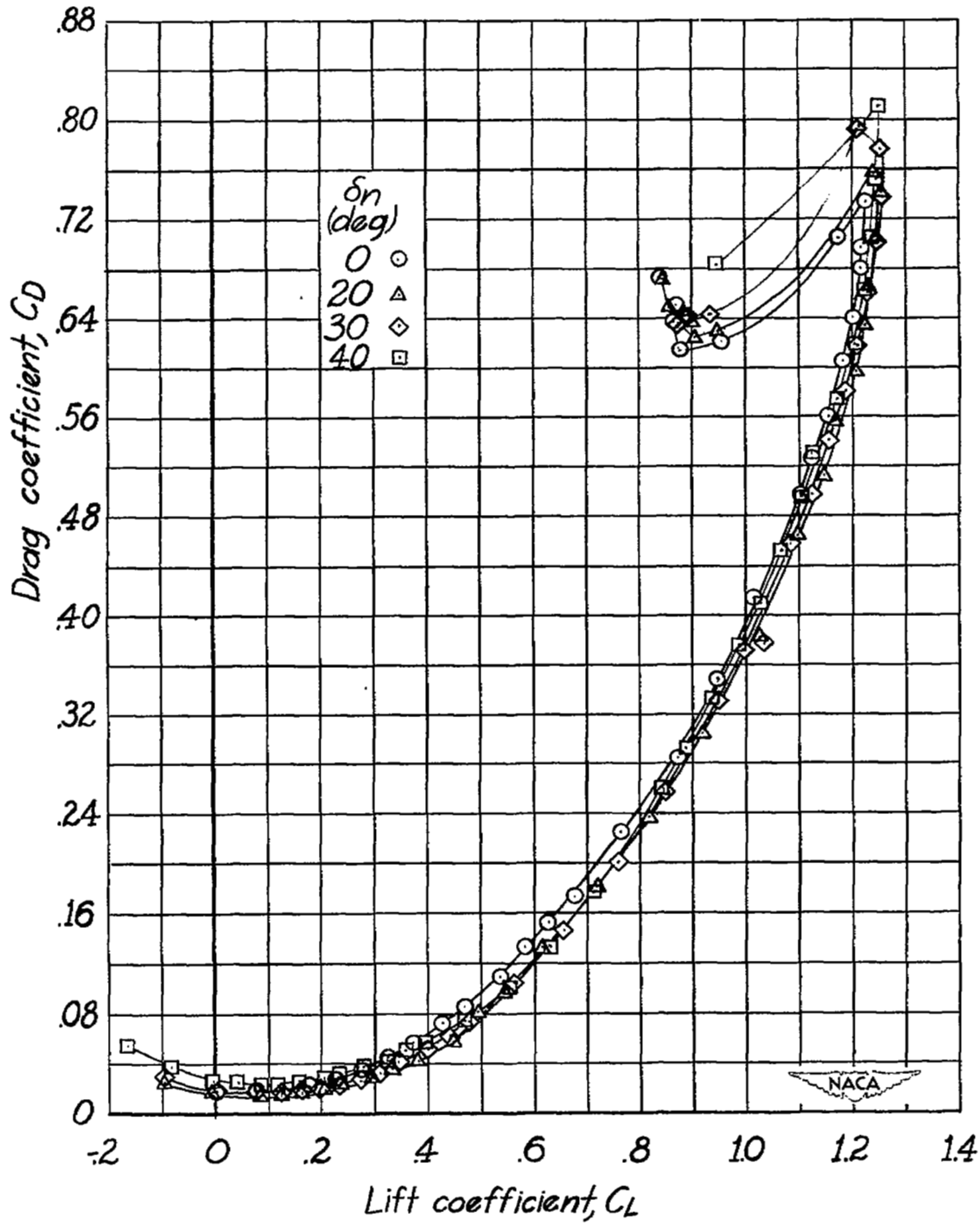

(b) Concluded.

Figure 5.– Concluded.

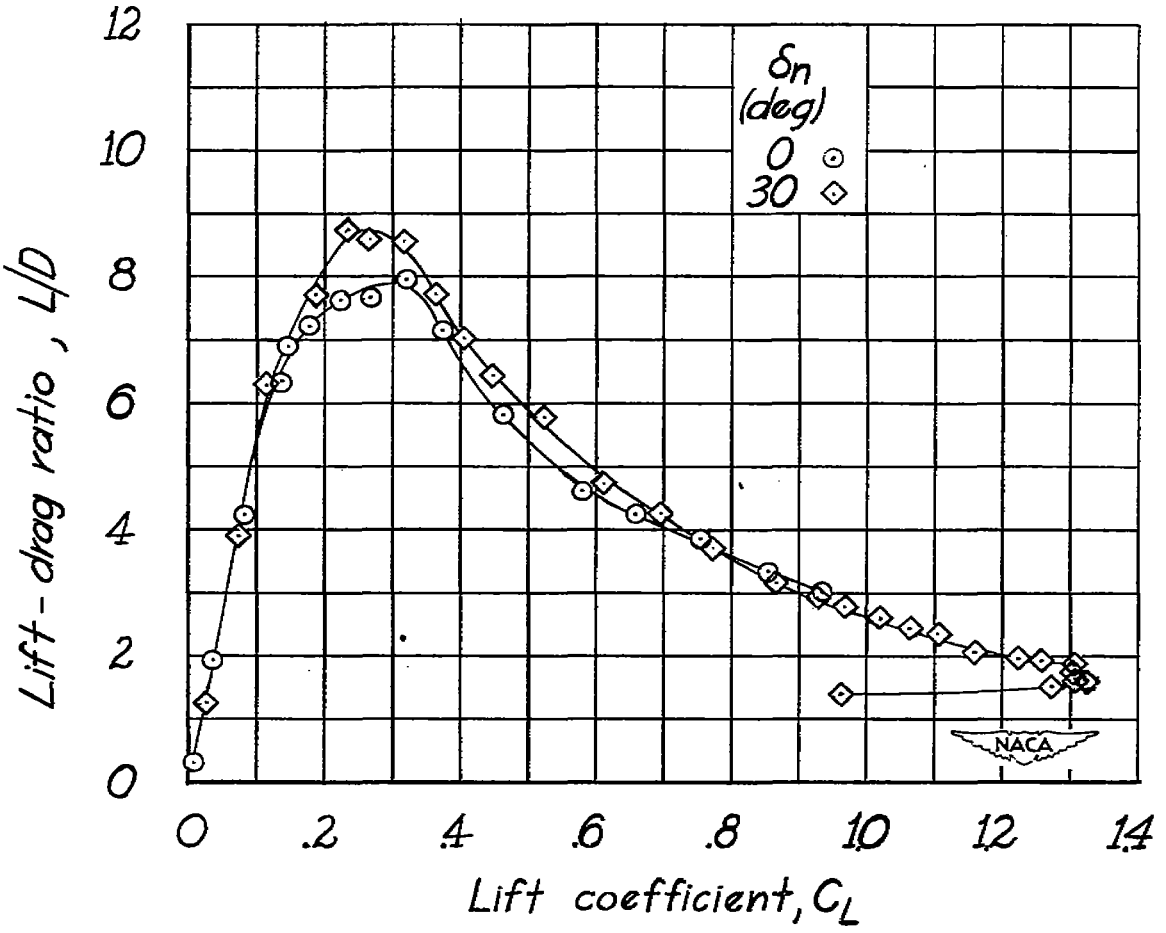

(a) $R \approx 1.5 \times 10^6$.

Figure 6.– Lift–drag ratios of 60° delta wing with full–span round leading–edge flaps.

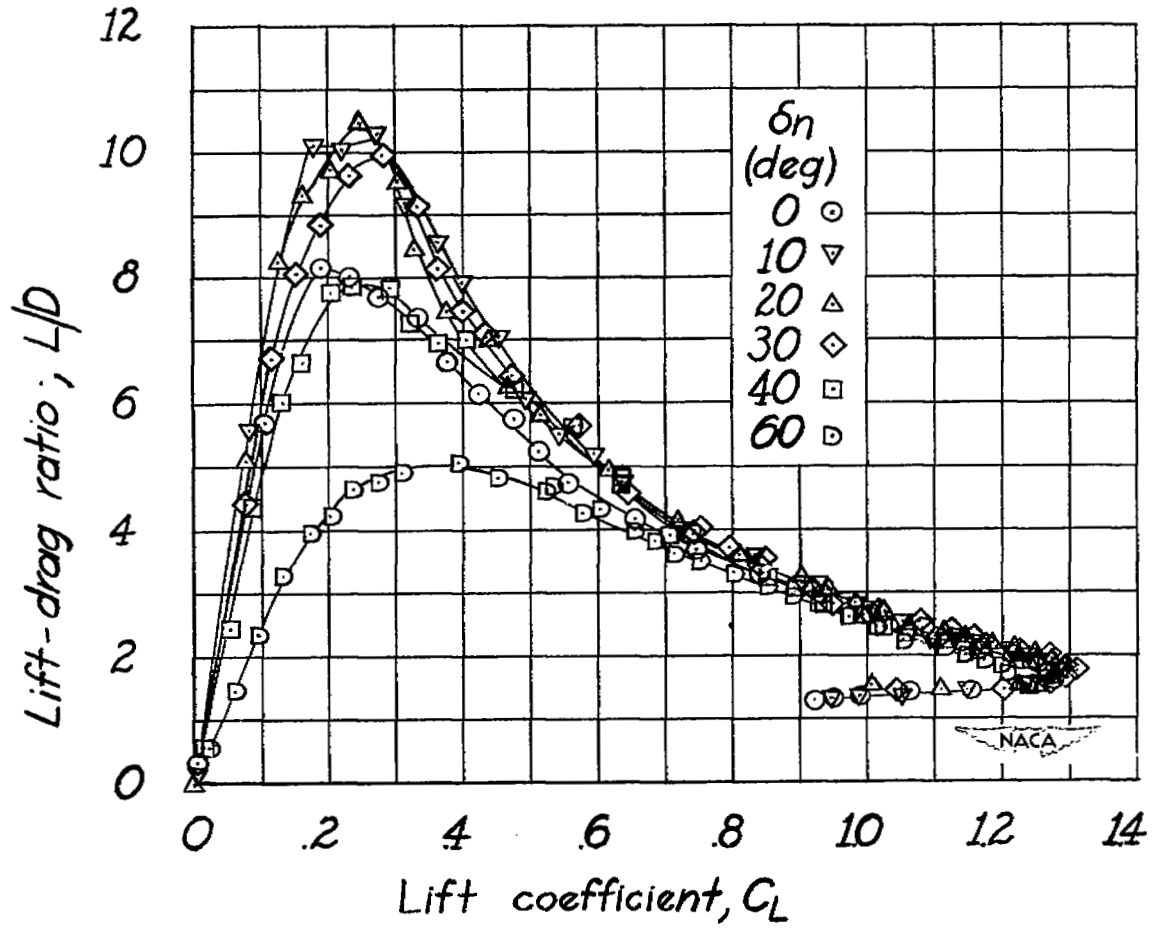

(b) $R \approx 3.0 \times 10^6$.

Figure 6.– Concluded.

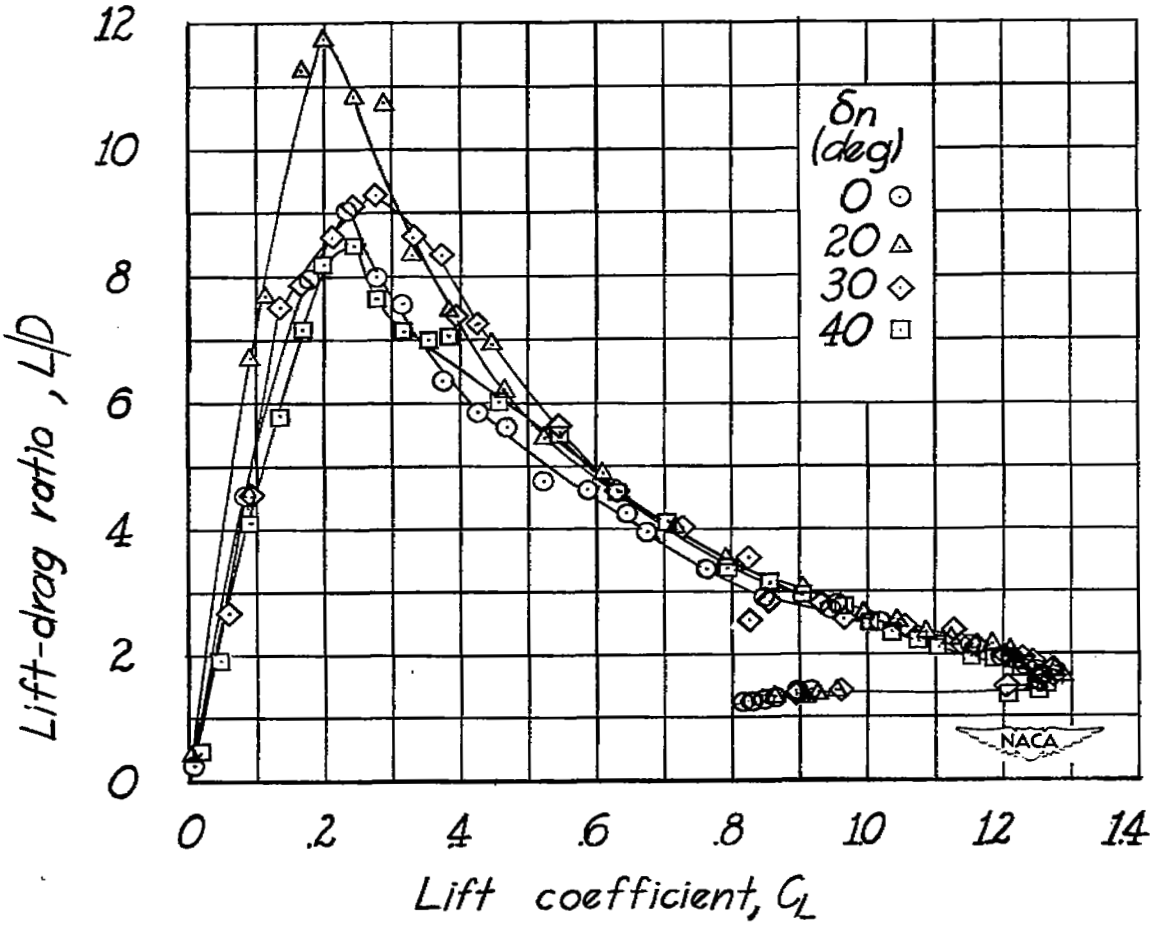

(a) $R \approx 1.5 \times 10^6$.

Figure 7.– Lift–drag ratios of 60° delta wing with full–span beveled leading–edge flaps.

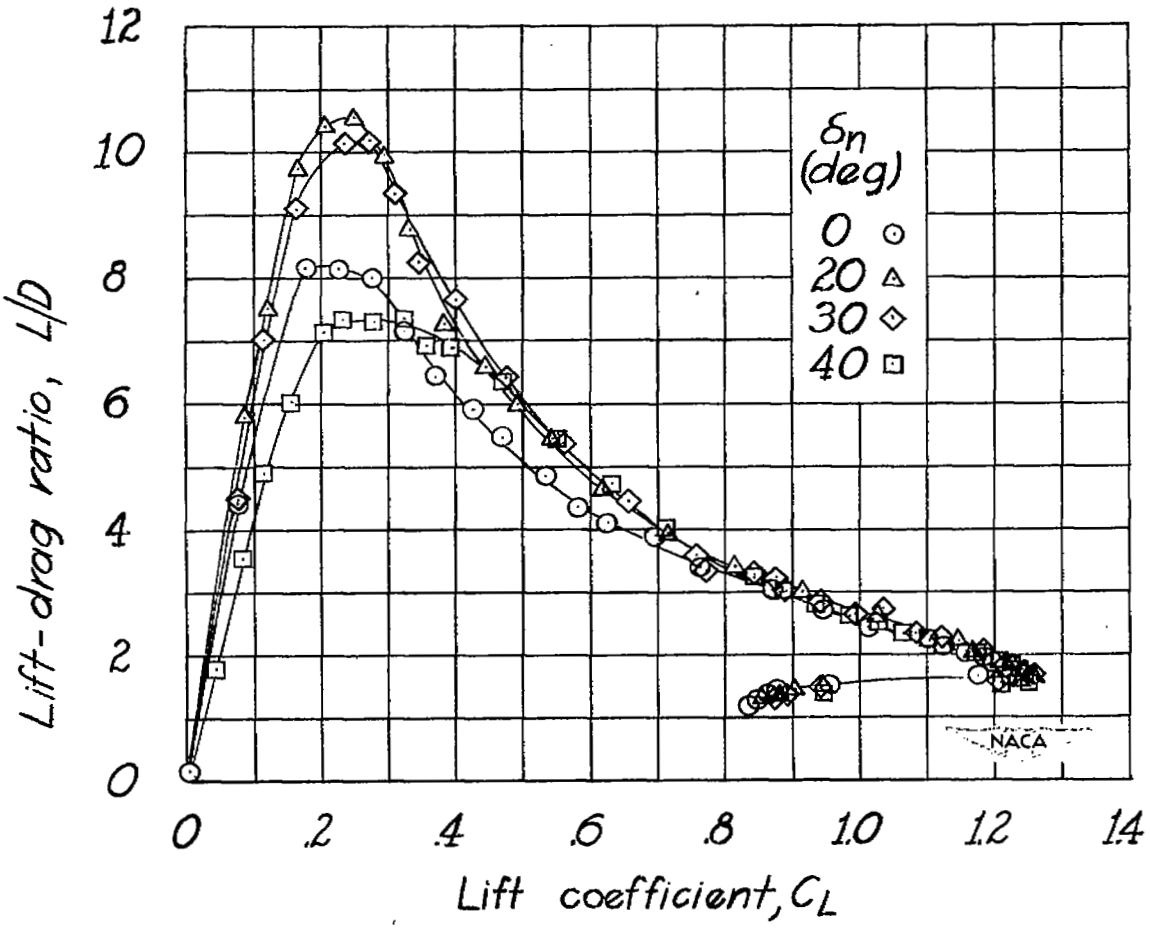

(b) $R \approx 3.0 \times 10^6$.

Figure 7.– Concluded.

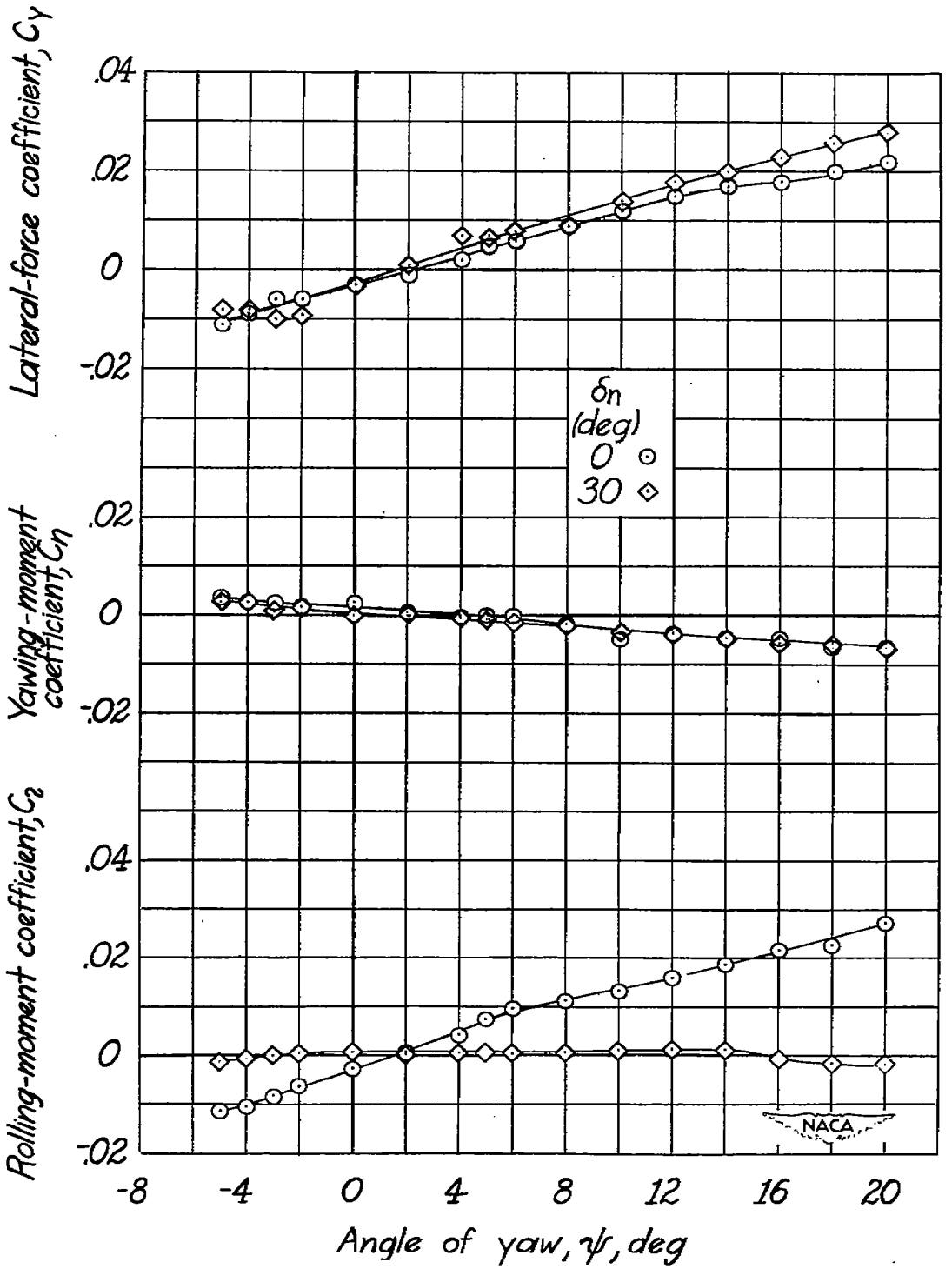

Figure 8.— Aerodynamic characteristics in yaw of 60° delta wing with full-span round leading-edge flaps; $\alpha = 10°$.

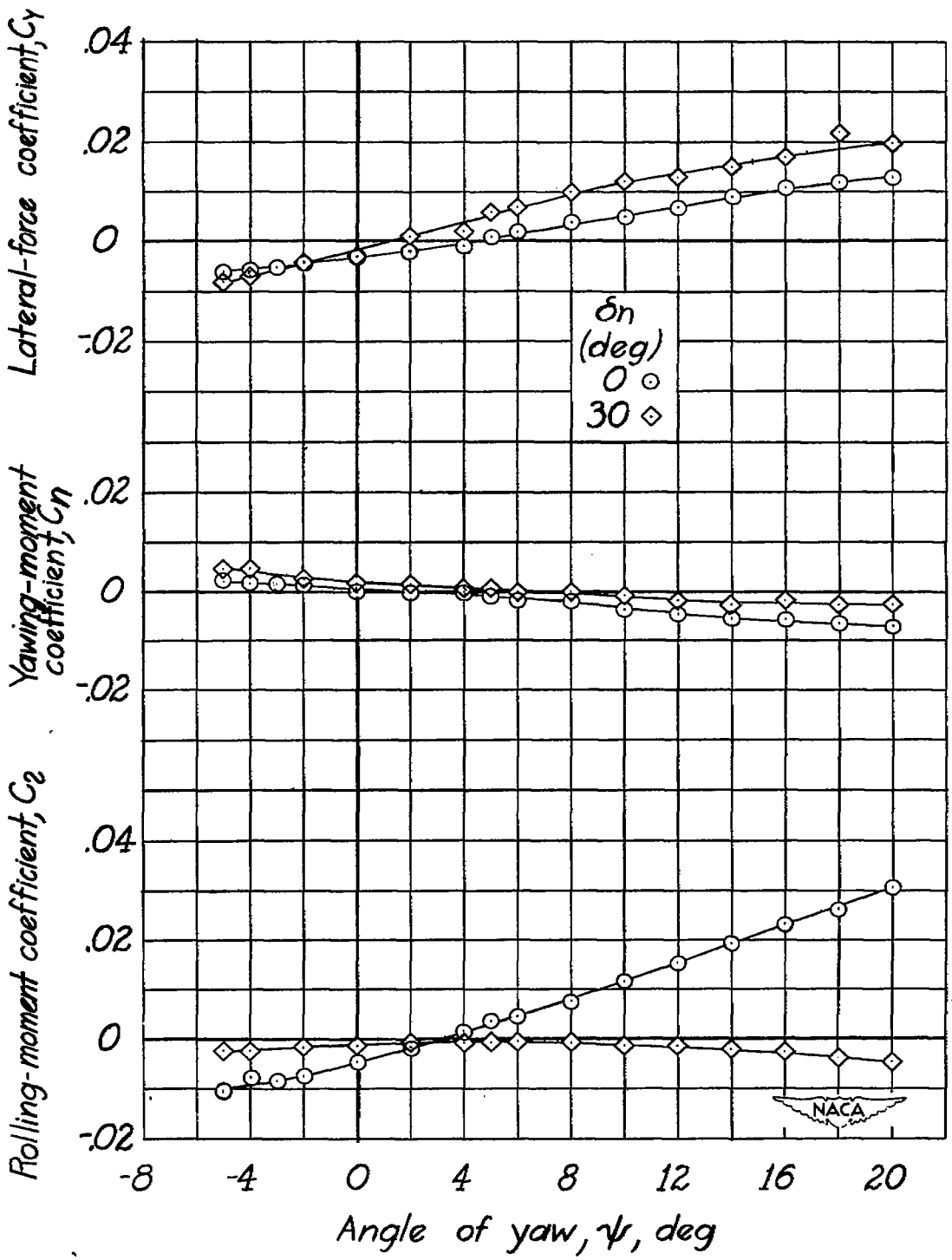

Figure 9.– Aerodynamic characteristics in yaw of a 60° delta wing with full-span beveled leading-edge flaps; $\alpha = 10°$.

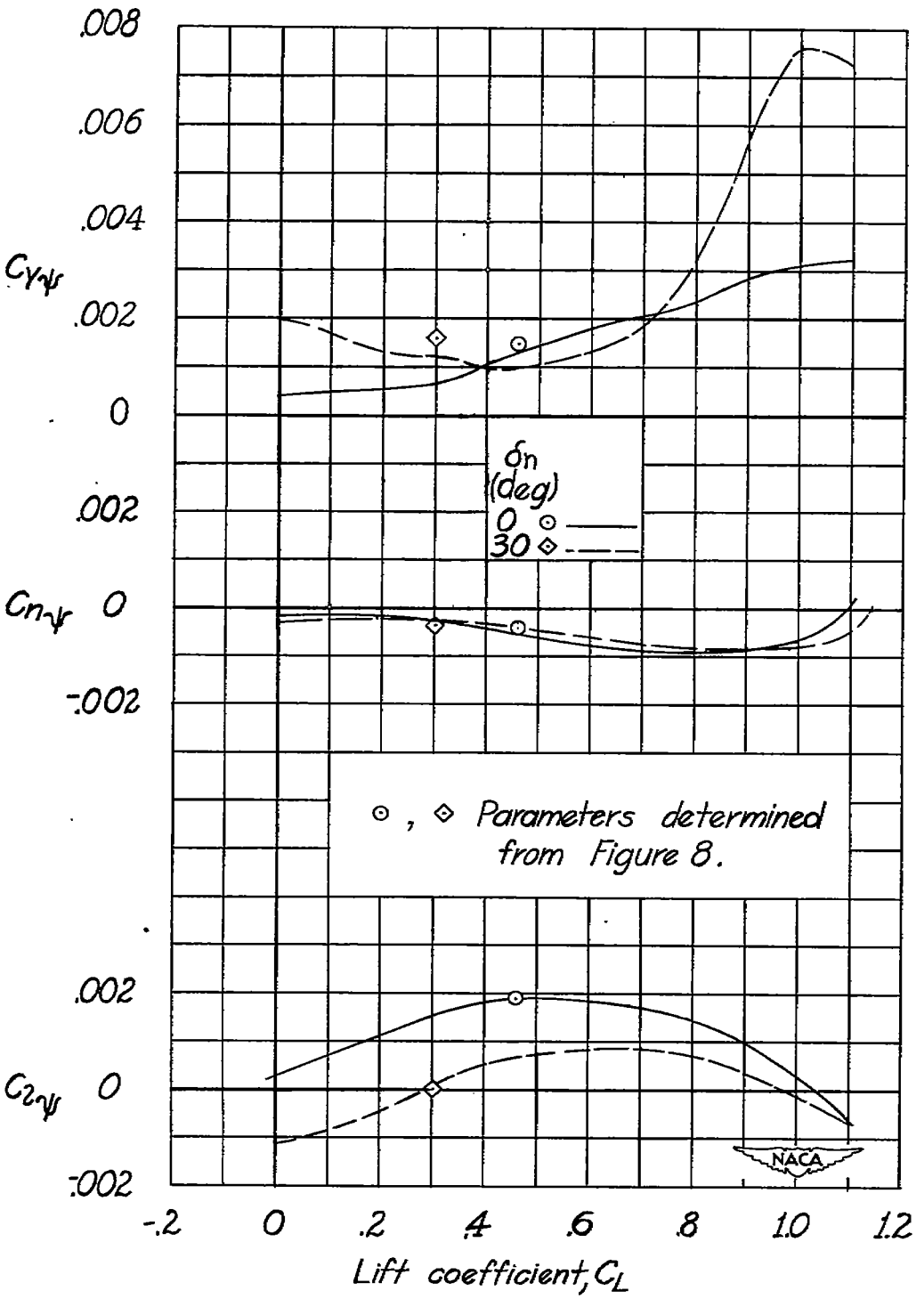

Figure 10.– The lateral-stability parameters of a 60° delta wing with full-span round leading-edge flaps.

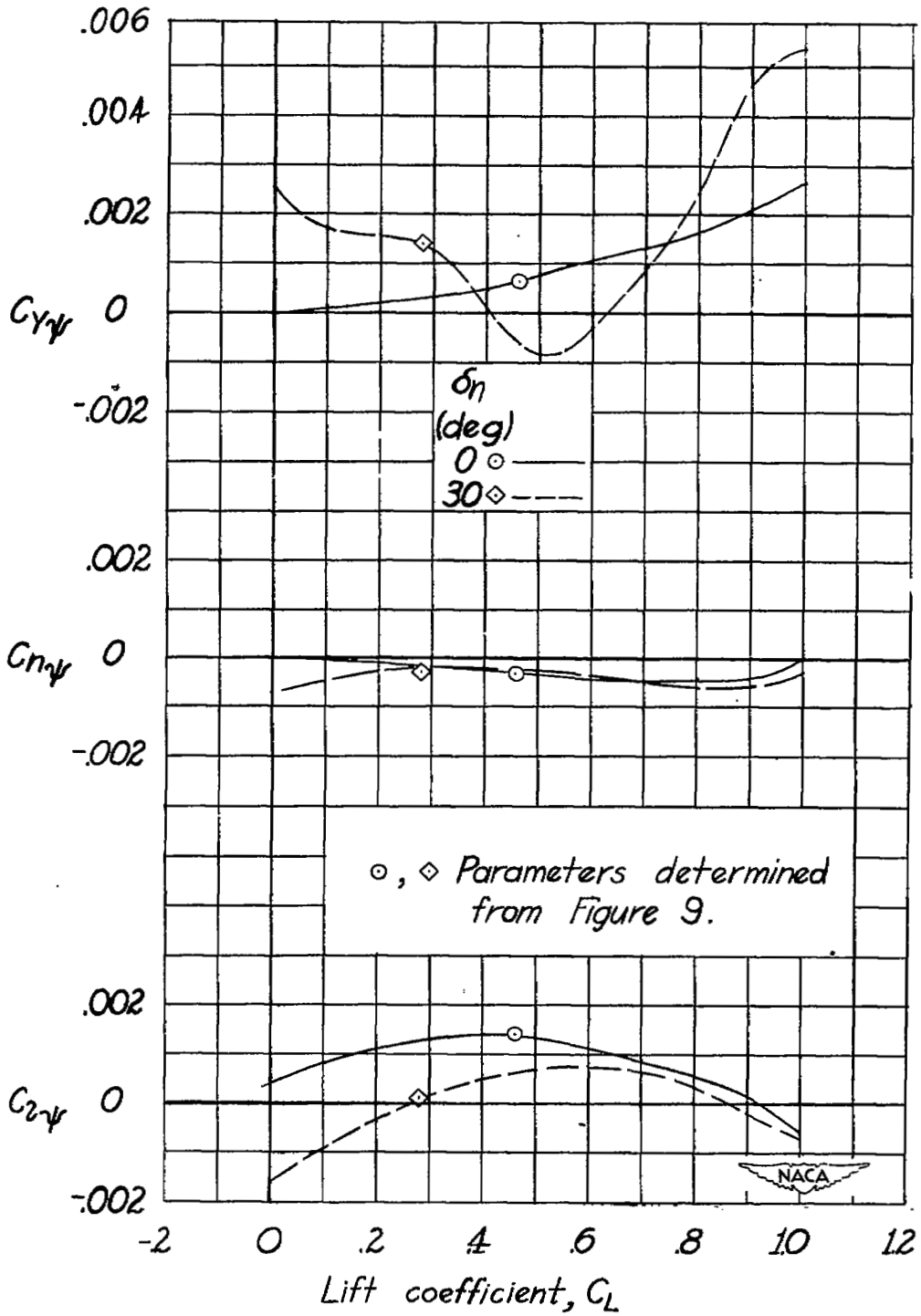

Figure 11.- The lateral-stability parameters of a 60° delta wing with full-span beveled leading-edge flaps.

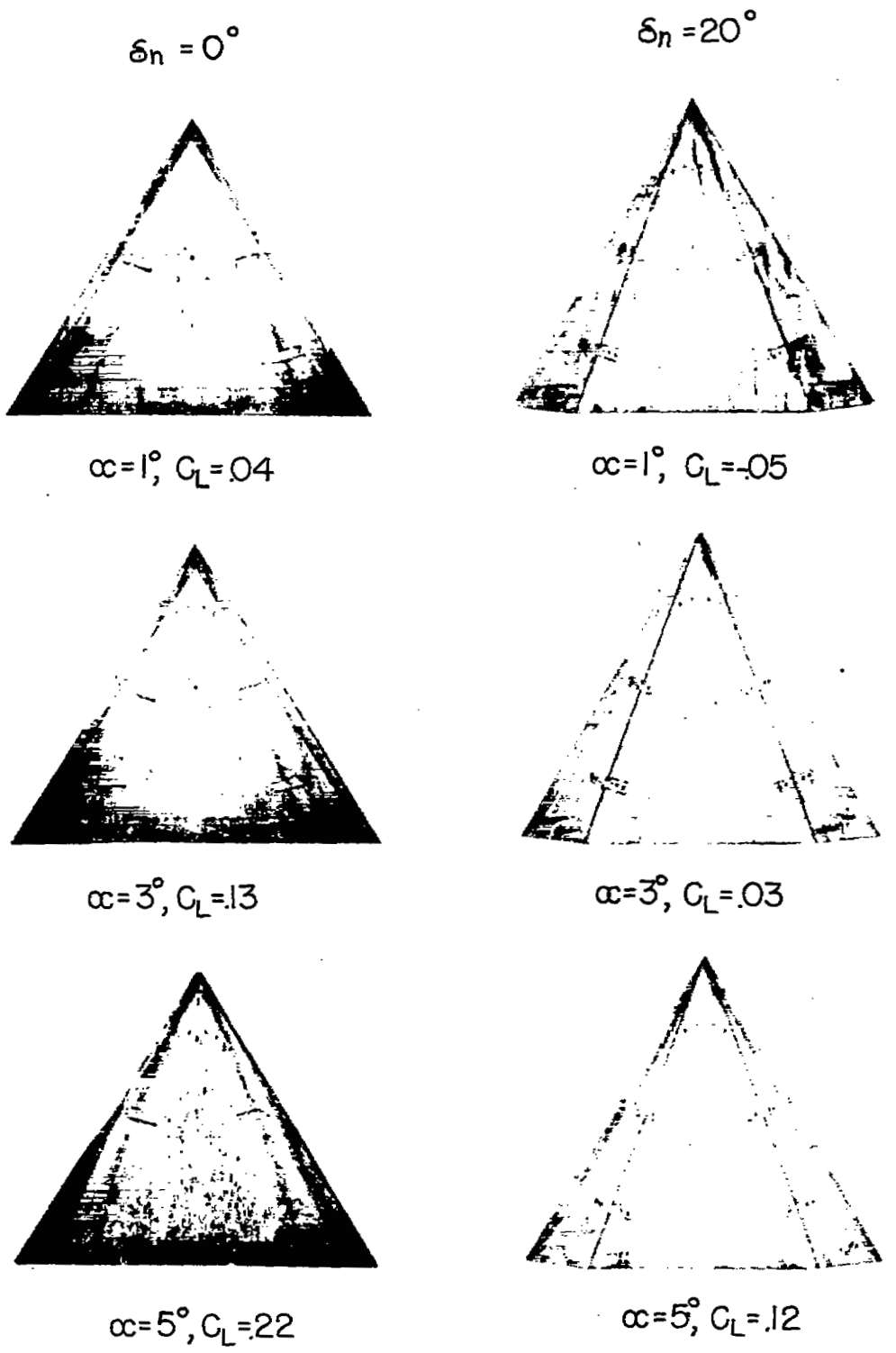

Figure 12.— Boundary-layer flow studies of 60° delta-wing model with full-span beveled leading-edge flaps.

$\delta_n = 0°$

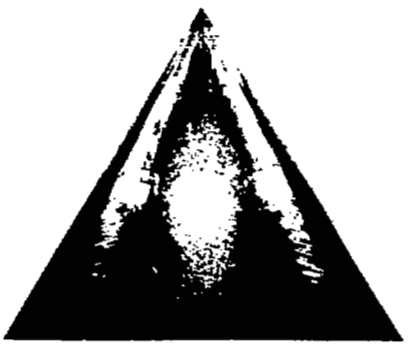

$\alpha = 8°, C_L = .36$

$\delta_n = 20°$

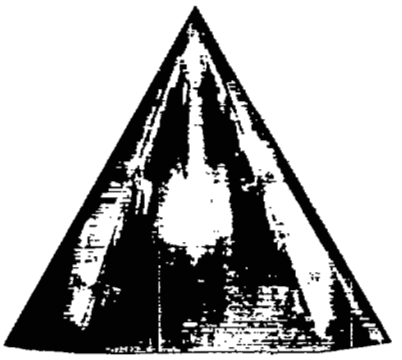

$\alpha = 8°, C_L = .24$

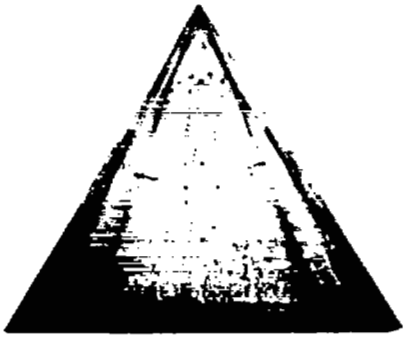

$\alpha = 8°, C_L = .36$

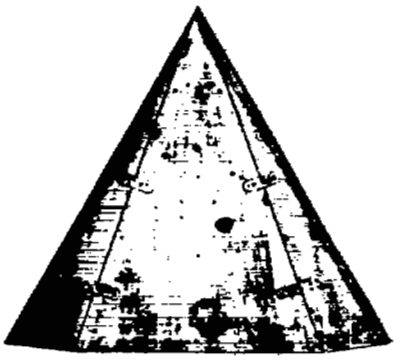

$\alpha = 8°, C_L = .24$

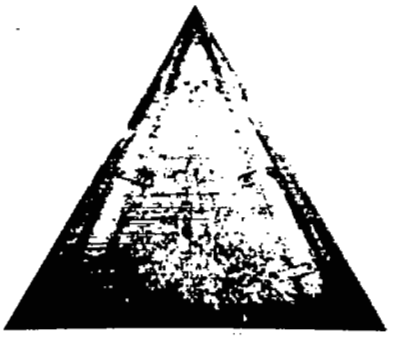

$\alpha = 16°, C_L = .76$

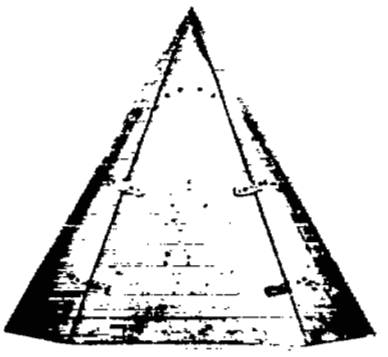

$\alpha = 16°, C_L = .62$

NACA L-60574

Figure 12.— Continued.

$\delta_h = 0°$

$\alpha = 20°, C_L = .93$

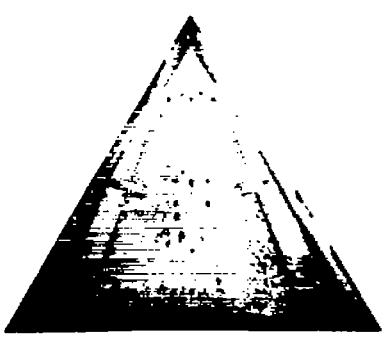

$\alpha = 20°, C_L = .93$

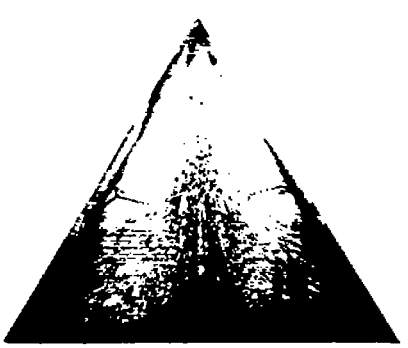

$\alpha = 25°, C_L = 1.12$

$\delta_h = 20°$

$\alpha = 20°, C_L = .81$

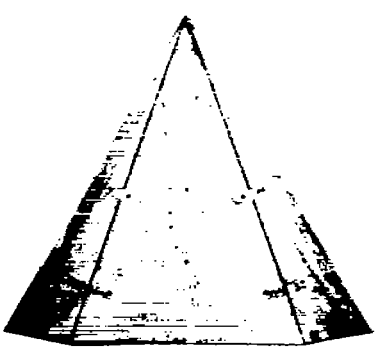

$\alpha = 20°, C_L = .81$

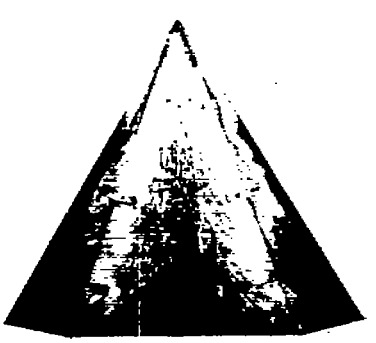

$\alpha = 25°, C_L = 1.05$

NACA L-60573

Figure 12.- Continued.

$\delta_n = 0°$

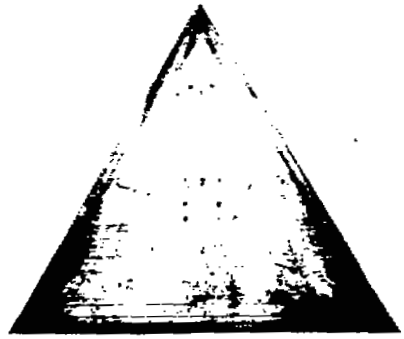

$\alpha = 25°, C_L = 1.12$

$\delta_n = 20°$

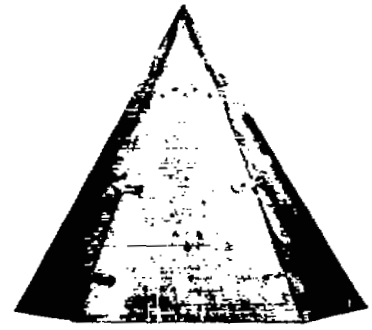

$\alpha = 25°, C_L = 1.05$

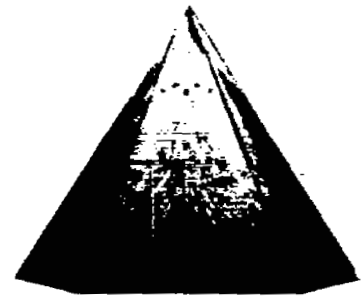

$\alpha = 35°, C_L = 1.14$

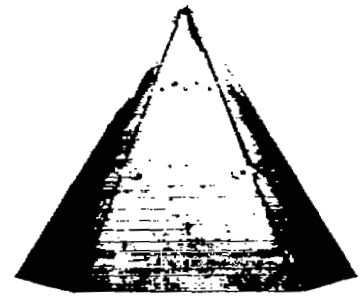

$\alpha = 35°, C_L = 1.14$

NACA L-60575

Figure 12.— Concluded.

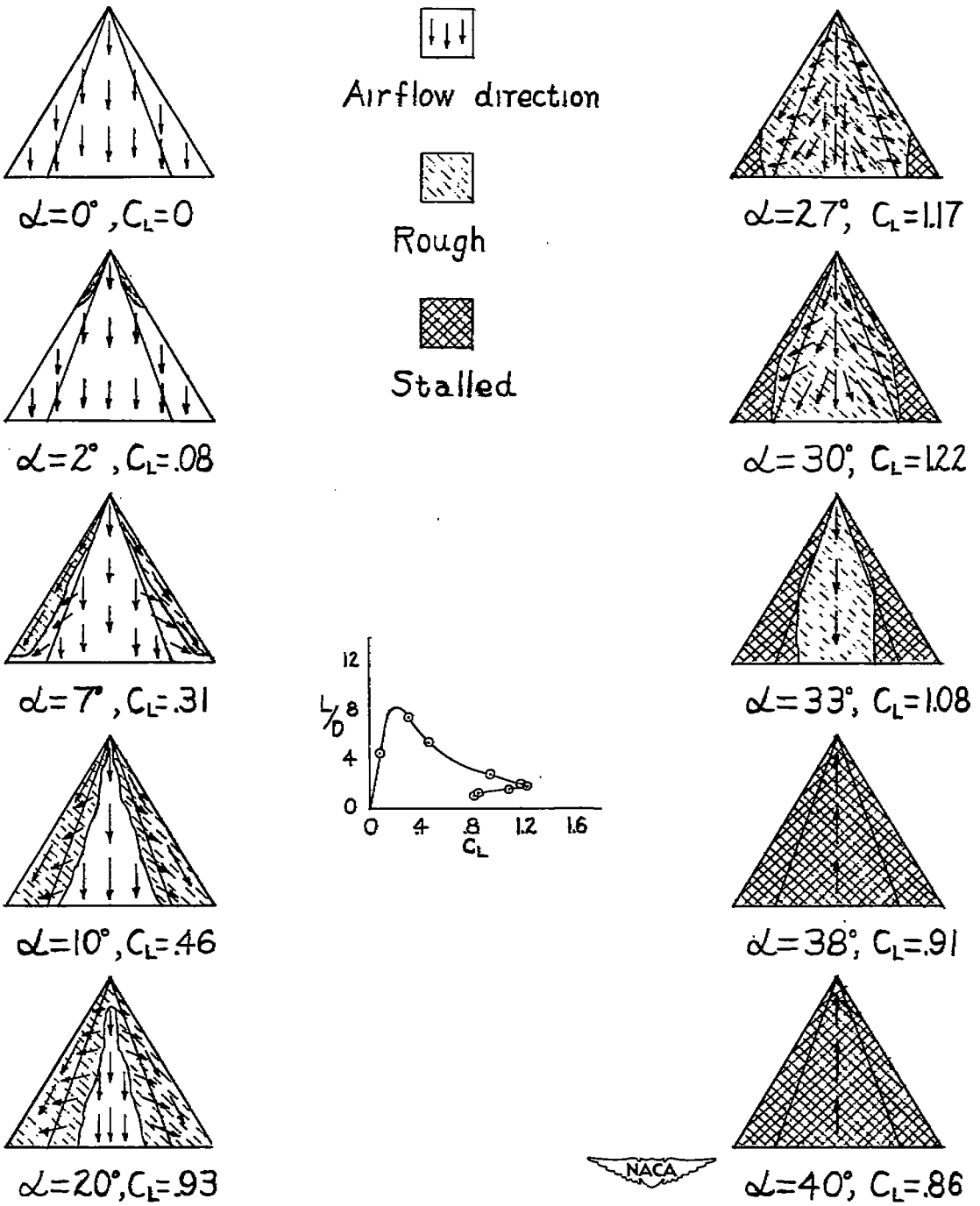

(a) $\delta_n = 0$.

Figure 13.– Stall studies of 60° delta-wing model with full-span beveled leading-edge flaps.

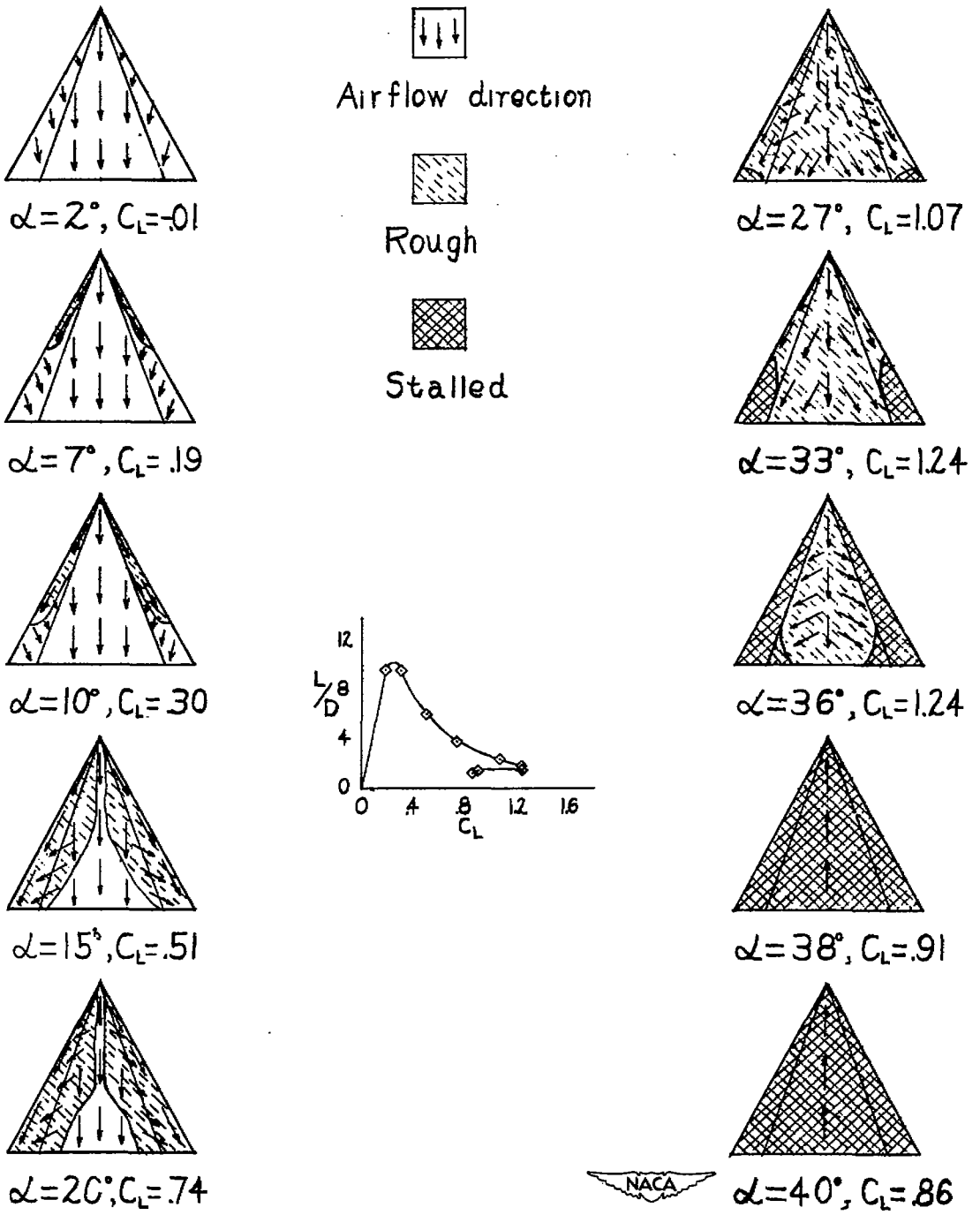

(b) δ_n = 30.

Figure 13.– Concluded.

NACA-Langley - 8-16-49 - 250